Contents

Introduction

The last years of scientific research have emphasized the study of the transport of aerosol in the atmosphere. The importance of knowledge of aerosol transport in the atmosphere is summarized in three main points:

1. direct influence on the radiative terrestrial balance; the particles of aerosol, like particles of cloud, reflect, absorb and transmit solar radiation. Aerosol particles have a substantial interaction with both solar and terrestrial radiation. The nature of such interactions depends on the total mass of aerosol (or water for clouds), the size and shape of droplets or particles, and their distribution in space.

2. indirect influence on the radiative terrestrial balance; aerosol particles are often the nucleus of aggregation for water droplets, which form a cloud that interacts with solar and terrestrial radiation.

3. influence on air pollution; the term "particles of aerosol" includes all kinds of polluting particles, such as SO_2 from vulcanos, Saharan dust, PM10, etc.

In order to investigate aerosol transport in the atmosphere there are two different appropriate methods: the use of transport models or experimental measurements. Currently there are many kinds of transport models and many typologies of experimental instruments, but the most accurate way to analyze the aerosol transport is a combination of both methods.

1. In the first chapter a brief introduction of the state of the art is presented:
   - section 1 deals with dispersion models
   - section 2 with experimental measurements
   - section 3 with the integration between them
2. In the second chapter the new Bol-Traj model created for this work is described:
   - section 1 explains its main characteristics
   - section 2 presents the numerical code.
3. The third chapter provides descriptions of the instruments used:
   - section 1 deals with the lidar of PEARL station of EARLINET NETWORK,
   - section 2 deals with CALIOP which is the lidar installed on CALIPSO,
   - section 3 describes the methodology used in order to convert the measurements from ground to space
   - section 4 furnishes a brief introduction to the MODIS satellite.
4. Finally, the fourth chapter illustrates three applications of the integration between numerical models and experimental measurements:
   - section 1 explains how the Bol-Traj model is useful for making a comparison between two instruments (CALIPSO and PEARL) that measure the same quantity in a different space-time reference,
   - section 2 shows how the application of the Bol-Traj model with the PEARL measurements allows the determination of the transport of SO_2 from the Etna volcano in the 2002 eruption,

- section 3 illustrates how the integration of information from the Bol-Traj model, PEARL, CALIPSO and MODIS measurements allows the estimation of the plume height of the forest fire in Algeria in August 2007.

Chapter 1

State of the Art

1.1 Aerosol transport models

The literature presents many kinds of different models. The first important point is to understand the difference between Eulerian and Lagrangian models. The major difference between them lies in their approach to the problem: in the Eulerian frame the particles are viewed as unmoving in the surrounding fluid, while in the Lagrangian frame they move with the fluid. The most important consequence is that the two different approaches are used for different aims. Eulerian transport is useful in order to know the concentration of aerosol at each point of a grid, as well as to make a comparison with experimental measurements if they are taken at a grid point, while Lagrangian transport supplies information on the history, origin and arrival of particles. A main advantage of Lagrangian models is that there is no artificial numerical diffusion as in the case of Eulerian models. This is of special importance in the vicinity of the source of an air pollutant, where in Eulerian models the pollutant is instantaneously mixed over at least one grid box, which can cause subsequent large transport errors.

1.1.1 Eulerian models

The Eulerian model solves the advection-diffusion equation for the aerosol concentration

$$\frac{\partial c}{\partial t} = \vec{u} \cdot \nabla c + \nabla^2 D c \tag{1.1}$$

This equation gives the variation in the time of the concentration at a fixed point determined by the velocity of the surrounding fluid, the cinematic diffusivity, turbulent dispersion and local sources of aerosol, which can be either actual pollution sources or chemical transformations. Let us write the components of velocity and concentration as mean values plus fluctuation

$$u_i = \langle u_i \rangle + u' \tag{1.2}$$

$$c = \langle c \rangle + c' \tag{1.3}$$

where $\langle c \rangle$ and $\langle u_i \rangle$ are the mean values and u' and c' the fluctuations. If the cinematic diffusivity is neglected, replacing the above quantities and making an average, the new advection-diffusion equation is obtained. A new unknown quantity appears in this equation, this being the correlation between fluctuations of velocity and concentration.

$$\langle c' u' \rangle \tag{1.4}$$

The term $\langle u_i \rangle$ is deduced from experimental measurements or from meteorological models, while the term $\langle c' u' \rangle$ must be determined. The latter term is expressed as a function of mean value, by means of an operation named "closure". Often the flux-gradient relation is assumed as closure

$$\langle c' u_i' \rangle = -k \frac{\partial \langle c \rangle}{\partial x_i} \tag{1.5}$$

where k is a constant. This hypothesis relates the correlation between the concentration fluctuations and the i-esima component of the wind, with the gradient along the direction of the i-esima component of mean concentration, in this

way closing the advection-diffusion equation. To solve the equation both analytical and numerical solutions are possible.

Grid models, for example, are numerical solutions of the advection-diffusion equation

$$\frac{\partial P(\vec{x})}{\partial t} = \vec{u} \cdot \nabla P(\vec{x}) + \nabla^2 D P(\vec{x}) \tag{1.6}$$

which is the same as (1.1), where concentration c is replaced by the probability of the vector position $P(\vec{x})$. The quantities are computed each time step of the model and are given at fixed points of space (grid points). Examples of important grid models are DREAM, used to predict Saharan events, and BOLCHEM.

DREAMS (Dust Regional Atmospheric Model) is a regional model designed to simulate and/or predict the atmospheric cycle of mineral dust aerosol, which currently represents the state of the art of Eulerian models for Saharan dust transport. It solves the Eulerian-type partial differential nonlinear equation for dust mass continuity eq (1.6). DREAM is fully inserted as one of the governing equations in the atmospheric NCEP/Eta atmospheric model. The concentration equation simulates all major processes of the atmospheric dust cycle. During model integration, calculation of surface dust injection fluxes is made over the model points declared as deserts. Once injected into the air, dust aerosol is driven by the atmospheric model variables: by turbulent parameters in the early stage of the process when dust travels away from the sources, and finally, by thermodynamic processes and rainfall of the atmospheric model and land cover features, which provide wet and dry deposition of dust over the Earth's surface. One of the key components of the dust model is the treatment of sourcing terms in the concentration continuity equation.

The BOLCHEM model (BOLam + CHEMistry) is the result of an on-line coupling between the mesoscale meteorological model BOLAM (BOlogna Limited

Area Model) and modules for transport and transformation of chemical species. Transport (advection and diffusion) of tracers (both passive and reactive) is performed on-line at each meteorological time-step using the WAF (Weighted Average Flux) scheme for advection and a "true"(second order) diffusion, with diffusion coefficient carefully estimated from experiments. Vertical diffusion is performed using a one-dimensional diffusion equation with a diffusion coefficient estimated by means of an E-l turbulence closure scheme. Dry deposition is computed through a resistance-analogy scheme and is provided as boundary condition to the vertical diffusion equation. Furthermore, the vertical redistribution of tracers due to moist convection is parameterised consistently with the Kain-Frisch scheme used in the meteorological part for moist convection. Transport of chemical species is performed in mass units, while gas chemistry is computed in ppm. Physical/chemical processes are treated separately for the gas phase, aerosol classes and generic tracers (e.g. radioactive species, Saharan dust, etc.). The gas phase is treated using the SAPRC90 or CB4 chemical mechanisms. Aerosol is modelled using the M7 module from ECHAM5 (coupling still in progress) and generic species are defined by the user, case by case, providing chemical/physical properties and equations.

1.1.2 Lagrangian models

In the Lagrangian model the frame of reference is movement with the surrounding fluid. Thus if $\vec{v}(t)$ is the velocity of the marker passive tracer and $\vec{u}(\vec{x}, t)$ is the flow velocity when the parcel passes at the point $\vec{x}$, the velocity is the same

$$\vec{v}(t) = \vec{u}(\vec{x}, t) \tag{1.7}$$

If it is supposed that the source is in $\vec{x}_0$ (initial position) and has an instantaneous release at time t_0 (initial time), the formal solution of the transport problem is

expressed by

$$\vec{x}(t) = \vec{x}(t_0) + \int \vec{v}(\tau) d\tau \tag{1.8}$$

If the velocity field is completely determined, equation (1.8) allows the computation of the position of the particles released from the source. In high Reynolds number flows, i.e. geophysical flows, this approach cannot be utilized. Firstly, measurements provide access only to some statistics of the fluid. Moreover, apart from direct numerical simulation, which can be performed in a restricted variety of conditions, any other numerical approach gives only a partial description of the velocity field. Thus, a stochastic approach must be adopted, giving a solution in terms of statistical proprieties of $\vec{x}$ resulting from equation (1.8). If it is supposed that the state of particles evolves as a Markovian process, different orders of the process are possible. In the free troposphere the velocity of the particles can be considered not correlated in time, because the time scale of the processes is greater than the Lagrangian correlation time. Therefore, after the typical time scale the state of parcel is determined only by the position. In this situation, the Markovian process is of "zero" order and is represented by the equation

$$d\vec{x}(t) = \vec{u}(\vec{x}(t), t)dt + \sqrt{2D}dW \tag{1.9}$$

where $\vec{u}(\vec{x}(t), t)$ is the velocity of the parcel at point $\vec{x}$ computed at time t, and the last part of the equation is the term of noise. The Lagrangian model that uses this equation is usually named "trajectories model". If it is necessary to understand processes in the planetary boundary layer, or processes like convection, where the scales of motion are smaller than in the FT (free troposphere), the above hypothesis on the decorrelation of the velocity is incorrect, because the typical time of the process is different. The time of such processes is less than the Lagrangian correlation time, but higher than the time of Kolmogorov τ, which is the time of correlation of acceleration. In this way, it can be considered that the acceleration is not correlated, while the velocity is correlated. For this reason the Markovian

order is "one" i.e. the state of particles is determined by the position and velocity. The equation becomes a system of two equations, one for transport and the other for the velocity field:

$$dx_i(t) = u_i dt \tag{1.10}$$

$$du_i(t) = a_i(\vec{x}, \vec{u}, t)dt + b(\vec{x}, \vec{u})dW_i \tag{1.11}$$

where dW is the white noise, ($W(t)$ is a Wiener process with a mean of zero and variance dt). In order to obtain the value of the velocity in the system of equations, it is necessary to determine $a(\vec{u}, t)$ and $b(\vec{x}, \vec{u})$. The expression for $b(\vec{x}, \vec{u})$ can be derived by the Kolmogorov theory on local isotropy in the inertial subrange

$$b(\vec{x}, \vec{u}) = C_0\epsilon \tag{1.12}$$

The expression for $a(\vec{x}, \vec{u})$ is derived from the Fokker-Planck equation:

$$\frac{\partial P}{\partial t} = -\frac{\partial a_i P}{\partial u_i} - \frac{\partial u_i P}{\partial x_i} + \frac{b^2}{2}\frac{\partial^2 P}{\partial u_i u_i} \tag{1.13}$$

where P is the density probability function of aerosol particles. By the well mixed condition the P is determined. The well mixed condition criterion (32) imposes that the density probability function of the aerosol particles after the time taken to reach the stationary condition is the same as that of the air particles. Usually, these kinds of models are called Lagrangian Particle Dispersion Models (LPDM).

An example of LPDM is FLEXPART, which is a model designed for operational emergency response and research applications. It simulates the long-range transport, diffusion, dry and wet deposition, and radioactive decay of air pollutants released at a location, or in backward mode, to determine the potential source contributions for a given receptor.

FLEXTRA is an example of a trajectory model, and it can be used to calculate different types of forward or backward trajectories. It is specifically

designed to compute long time sequences of trajectories for many receptor locations. FLEXTRA is currently based on model level data of the numerical weather prediction model of the European Centre for Medium-Range Weather Forecasts (ECMWF). Gridded data of this model are available at various horizontal resolutions, 31 vertical levels, with a frequency of 3 hours. FLEXTRA is based on gridded meteorological fields (analyses or forecasts) from the numerical weather prediction model of the European Centre for Medium-Range Weather Forecasts, given in a latitude/longitude coordinate system. It is a stochastic model and can to be driven by global or regional meteorological models.

HYSPLIT (HYbrid Single-Particle Lagrangian Integrated Trajectory model) is a trajectory model, whose classification is used to identify the role exerted by meteorology on air quality in the Naples urban area (Southern Italy) (3). The trajectories obtained from ensemble simulations have been classified by a combination of the k-means and PCA (Principal Component Analysis) approaches.

1.1.3 Hybrid models

In some cases it is necessary to use both Eulerian and Lagrangian approaches. For example, when it is important to know the concentration of aerosol arriving in a region of space from a source that is smaller than the Eulerian model box grid, it is useful the employ a hybrid model.

A few representative examples of this kind of model are DREAM (Danish Rimpuff and Eulerian Accidental release Model) (2), which has the same name as that of Eulerian model presented above, the “folded retroplume model” and the “Lagrangian model using Eulerian passive tracers”.

The first is created in order to study transport, dispersion and deposition,

on large or small scales, of radioactive pollution arriving from single but intense sources, such as Chernobyl. Near the source, a Lagrangian approach is used to better describe the source, without the diffusion typical of the Eulerian model, while far from the source, at larger scale, a Eulerian transport should be used. The transport is driven by a mesoscale meteorological model.

The purpose of the second model is to provide a way to determine efficiently and accurately the transport pathway of emissions to receptor, highlighting only those emissions that arrive in the receptor cell at the time of interest, using standard gridded (Eulerian) output fields from an LPDM. This can be accomplished by combining the standard output from a forward model simulation with that from a backward simulation, bringing the information from the forward and backward models together in such a way that even complex transport scenarios can be analysed.

The "Lagrangian model using Eulerian passive tracers" is a method for tracking coherent Lagrangian airmasses not based on the computation of individual trajectories, but rather on three Eulerian passive tracers initialized with the coordinates of each grid cell. This initial coordinate method allows the later unambiguous identification of each Lagrangian air parcel by referring to its initial position. The Lagrangian description of a flow consists of identifying any fluid parcel at any moment without ambiguity. With trajectories the identification is evident since the parcel location is know at any time (12).

1.2 Experimental Aerosol measurements

1.2.1 LIDAR

The LIDAR equation

Lidar is an acronym for LIght Detection And Ranging. It is used for many applications: to study stratospheric and tropospheric aerosol and cloud, and to determine the vertical profile of water vapour, H_2O, O_3, CH_4, NO_x, temperature and other atmospheric constituents. It is based on a special system that sends a laser pulse beam into the atmosphere. Each laser pulse interacts with the atmosphere, so that a portion of the energy sent is backscattered and detected by a telescope. This radiation is selected by wavelength and sent to a receiver system that emits electric signals proportional to the optical power received. Because the laser beam has the speed of light in the atmosphere, evaluating the time between laser emission and the detection, the distance of the target is estimated and so the profiles of atmospheric parameters as a function of the height are estimated too. The interaction between the laser radiation and atmospheric constituents is manifold: elastic and anelastic scattering, absorption or ri-emission with fluorescence are possible. The equation of the lidar depends on the kind of process investigated. For the present purpose a monostatic lidar is considered (19), i.e. a lidar with the transmitter and receiver positioned in the same space, and it is assumed that it is a process of single elastic or anelastic scattering, keeping in mind the correction for multiple scattering if needed. The optical power $P(\lambda, \lambda_L, R)$ received by the receiver, in the spectral interval $(\lambda, \lambda + \delta\lambda)$, for the parcel of atmosphere located in r in the interval of height $(R, R + \delta R)$ the volume of which is individualised by the area of the laser beam at the height of R and width δR is:

$$P(\lambda, \lambda_L, R) = \int J(\lambda, \lambda_L, R, r)\delta\lambda\delta R p(\lambda, R, r) dA(R, r) \tag{1.14}$$

where λ is the wavelength detected, λ_L is the wavelength of the laser source, $J(\lambda, \lambda_L, R, r)$ is spectral radiance at λ wavelength induced by laser radiation (λ_L) at the position r in the normal plane to the direction of propagation, located at distance R for unit distance interval; $\delta\lambda$ is the band width of the radiation observed; $p(\lambda, R, r)$ is the probability of the radiation of λ wavelength coming from $dA(R, r)$ to strike the receiver; $dA(R, r)$ is the element of area of the atmospheric region located in the position r at distance R. The term $p(\lambda, R, r)$ includes different factors: geometric factors, phenomena of atmospheric attenuation and optical properties of the receiver and the system of spectral selection. The "Compact form" of the equation is written:

$$p(\lambda, R, r) = \frac{A_0}{R^2} T(\lambda, R)\zeta(\lambda)\chi(R, r) \tag{1.15}$$

where $\frac{A_0}{R^2}$ is the solid angle of acceptance of the receiver with A_0 the area of the telescope lens; $T(\lambda, R)$ is the atmospheric trasmissivity at λ wavelength and at altitude R, $T(\lambda, R) = e^{-\int \alpha(\lambda, R')dR'}$ where $\alpha(\lambda, R')$ is the extinction coefficient, defined as the reduction of the energy flux in the unit of travel in the direction of propagation that includes absorption and scattering; $\zeta(\lambda)$ is the spectral response of the receiver system at λ wavelength; $\chi(R, r)$ is the "overlap function", representing the probability of the radiation coming from r, at distance R to arrive at the receiver, supposing that this probability depends only on the superimposition of the laser beam with the receiver's field of view. The spectral radiance term $J(\lambda, \lambda_L, R, r)$ depends on the interaction between the laser beam and the atmosphere (19). In the case of scattering:

$$J(\lambda, \lambda_L, R, r) = \beta(\lambda, \lambda_L, R, r)I(\lambda_L, R, r) \tag{1.16}$$

where $I(\lambda_L, R, r)$ is the laser irradiance, i.e. the laser energy flux in the unit of area and time, at position r at distance R at λ wavelength; $\beta(\lambda, \lambda_L, R, r)$ is the backscatter coefficient, i.e. quantity of incident energy backscattered in the unit of solid angle and atmospheric thickness. Integrating the equation for the

optical power $P(\lambda, \lambda_L, R)$ over the spectral window, and replacing the expression for spectral radiance and probability, the equation becomes:

$$p(\lambda, \lambda_L, R) = \delta R \frac{A_0}{R^2} \int \zeta(\lambda) d\lambda \int \beta(\lambda, \lambda_L, R, r) I(\lambda_L, R, r) T(\lambda, R) \chi(R, r) dA(R, r) \tag{1.17}$$

If it is assumed (19) that the line widths of the laser radiation and backscattered radiation are very small, and that they have the same scale, then the backscatter coefficient and the atmospheric trasmissivity are delta function with respect to λ. If it then assumed that the spatial distribution of laser intensity is uniform over the area A, and that the superimposition factor $\chi(R, r)$ is 1 where the receiver's field of view is superimposed over the laser beam and zero elsewhere (if this hypothesis is not valid, special correction is required), then the lidar equation becomes:

$$p(\lambda, \lambda_L, R) = \delta R \frac{A_0}{R^2} \zeta(\lambda) \beta(\lambda, \lambda_L, R) I(\lambda_L, R) T(\lambda, R) A(R) \tag{1.18}$$

If it is also considered that the laser pulse is rectangular and lasts τ_L, the equation becomes:

$$p(\lambda, \lambda_L, R) = P_L \delta R \frac{A_0}{R^2} \zeta(\lambda) \beta(\lambda, \lambda_L, R) T(\lambda, R) T(\lambda_L, R) \tag{1.19}$$

In this equation δR is the thickness of the atmospheric parcel considered i.e. the vertical resolution. To determine exactly the vertical resolution, the characteristic times must be considered:

1. τ_L is the time taken by the laser pulse to cover the distance between transmitter and receiver

2. τ_i is the time of interaction between photon and air parcel

3. τ_d is the time of resolution of acquisition of the system

Because $\tau_i << \tau_d$ and $\tau_L << \tau_d$, then $\delta R = c\tau_d/2$ and the final equation of the lidar is:

$$p(\lambda, \lambda_L, R) = P_L \frac{c\tau_d}{2} \frac{A_0}{R^2} \zeta(\lambda) \beta(\lambda, \lambda_L, R) T(\lambda, R) T(\lambda_L, R) \tag{1.20}$$

The equation is correct in the case of single scattering. Multiple scattering must be considered in the case of cloudy or foggy skies, because after scattering some photons change their direction with respect to that of the laser beam, but can return after other scattering phenomena.

LIDAR for the atmospheric aerosol study

The LIDAR equation changes as the interaction changes in the atmosphere between laser radiation and air particles, so that different configuration allow to investigate different atmospheric components. Usually, the DIAL technique is useful to determine concentrations of CO_2, NO_x, O_3, CH_4 and other kinds of pollution. The Raman technique is useful to study water vapour, and the elastic lidar configuration is suitable for atmospheric aerosols. In the elastic configuration (19) the substitution $\lambda = \lambda_L$ is valid, so that the lidar equation becomes:

$$p(\lambda_L, R) = P_L \frac{c\tau_d}{2} \frac{A_0}{R^2} \zeta(\lambda_L) \beta(\lambda_L, R) e^{-2\int \alpha(\lambda_L, R')dR'} \tag{1.21}$$

Here, the elastic backscatter coefficient β and the extinction coefficient α appear. Both parameters contain information on the concentration, distribution and optical proprieties of the atmospheric particles. The parameters depend on dimension, shape and composition of particles. For this reason they are linked and the lidar equation has two unknown variables. Very often it is not possible to have different measurements of the two parameters so, in this case, a quantity, named *lidar ratio* is supposed. This quantity permits to obtain the equation with just one unknown variable, because it is the ratio between the aerosol extinction coefficient and aerosol backscatter coefficient Since the lidar ratio depends on the kind of aerosol but not on the quantity, to suppose a value for it means to suppose the chemical-physical characteristics of the atmosphere. In order to solve this problem, it is possible to provide the lidar receiver system with a channel to capture data of backscatter radiation by Raman effect, for a gas whose quantity in the atmosphere is known,

such as nitrogen. In this condition the lidar equation becomes:

$$p(\lambda, \lambda_L, R) = P_L \frac{c\tau_d}{2} \frac{A_0}{R^2} \zeta(\lambda)\zeta(\lambda_L) N(R) \sigma_{\mathrm{R}am}(\lambda, R) T(R, \lambda) T(R, \lambda_L) \qquad (1.22)$$

where $N(R)$ is the concentration at altitude R of the molecule considered. A lidar system with combined elastic-Raman technique provides independent extinction and backscatter measurements.

1.3 Integration between theoretical models and experimental measurements

The introduction has already highlighted the importance of improving knowledge of aerosol transport, as well as the utility of using different methods. The best approach, as mentioned, is to integrate experimental measurements and theoretical models. It is possible:

1. to have an interpretation of experimental measurements using numerical simulations
2. to improve the parameterization of the model using the comparison with experimental measurements
3. to assimilate data in the numerical models.

Currently, integration between models and measurements is used to obtain a better knowledge of transport events. In (34), for example, the FLEXPART model and GOME instrument are employed to describe intercontinental transport of nitrogen oxide pollution plumes, while in (33) different kinds of aerosols detected by the lidar of the Potenza EARLINET station are explained by a transport model. A further example is supplied in (4), where the aim is to investigate the transport of SO_2 emitted from the Hekla volcano in the eruption of 17 August 1980, making use

of satellite measurements on UV and IR wavelength in the platform NOAA TOVS (TIROS Operational Vertical Sounder). The origin of the aerosol detected by the satellite is investigated by backward and forward trajectories of the HYSPLIT model (8)

Chapter 2

The Bol-Traj model

2.1 Theoretical model

Theoretical models are important tools for investigating the transport of atmospheric aerosols in a 4-dimensional structure. They give a more complete idea of the displacement in space-time than measured data. In particular, trajectory models are useful for studying transport phenomena in the atmosphere. In the environmental sciences, they are often employed to establish source-receptor relationships among air pollutants. Numerous trajectory models are described in the literature, but few offer the flexibility and broadness ideally required by the user. In this work, a new dispersion model (trajectories model) is created, Bol-Traj. Bol-Traj is an acronym for BOLAM, the name of a meteorological code that is the driver program that already exists, and Trajectories, which is the new dispersion model. The BOLAM dynamics is based on hydrostatic primitive equations, with wind components, potential temperature, specific humidity, and surface pressure, as dependent variables. The vertical coordinate system is hybrid-terrain-following, with variables distributed on a non-uniformly spaced, staggered Lorenz grid. The horizontal discretization uses geographical coordinates on an Arakawa C-grid. The time scheme is split-explicit, forward-backward for gravity

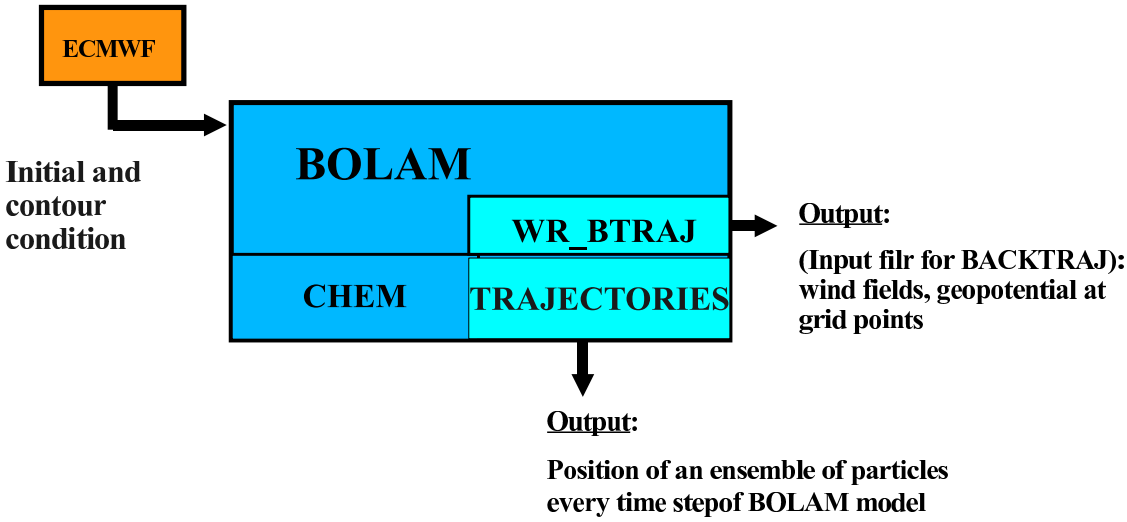

Figure 2.1: flow chart of forward trajectories

modes. A 3-D WAF advection scheme coupled with semi-Lagrangian advection of hydrometeors is implemented. A fourth order horizontal diffusion of the prognostic variables (except for Ps), a second order divergence diffusion and damping of the external gravity mode are included. The lateral boundary conditions are imposed using a relaxation scheme that minimises wave energy reflection. The initial and lateral boundary conditions are supplied by the ECMWF (European Centre for Medium-range Weather Forecasts) analyses available at 0.5 x 0.5 or 0.25 x 0.25 degree resolution. Hybrid model-level data are directly interpolated on the BOLAM grid. Trajectories is a Lagrangian dispersion model, and therefore implements the differential stochastic equation 1.9 in the numerical code. The different models are connected as represented in the figure 2.1 The model Traj and CHEM are interfaced with BOLAM because they run on-line with it.

The main characteristics of Trajectories are:

- it is a Lagrangian dispersion model; it is useful to know the history of the

particles released at a chosen space-time point.

- it uses a differential stochastic equation 1.9; it is applicable in Free Troposphere

- it adopts the numerical method of Eulero

$$f(t) = f(t_0) + \dot{f}(f(t_0), t_0)(t - t_0) \tag{2.1}$$

- it uses 3-D linear interpolation of these meteorological values on grid points in order to find the value at any point in space

- it can be used forwards or backwards in time; "forward mode" establishes where the particles released are moving to, while "backward mode" indicates where they are coming from

- in backward mode, the model uses linear interpolation in time of meteorological fields saved in an output file of wr_btraj, in order to obtain the value at each time desired. The backward trajectories are not computed on-line with the meteorological model, because it is necessary to save all the wind fields in an output file in order to use this file as input to compute the backward trajectories, inverting the sign of the time. For this reason, it is necessary to choose the time passing between the two fields saved. To compute the back-trajectories, it is necessary to choose the time of each time step of the model, while to obtain the wind fields at the time chosen, the meteorological fields saved in the file must be interpolated.

- it is possible to use deterministic or stochastic trajectories (if the term of the diffusion D in the equation 1.9 is "zero" the trajectories are deterministic)

- subroutines must be written for the origin and destination of trajectories; the model is constructed to be applicable for any case study, with any typology of

particle source as trajectory start, and any typology of trajectory destination. Therefore, it is necessary to develop an appropriate scheme that represents the origin and another for the destination of the trajectories, and to write the relative subroutines.

2.2 The Bol-Traj code

The numerical code of the Lagrangian dispersion model, called Bol-Traj, is created in this work. The structure of the code is divided into subroutines. This characteristic permits the use of the model in different cases, as well as the insertion of different kinds of aerosol sources and the use of the same code `Trajectories.F90` in forwards or backwards mode in time. There are some differences in the forwards or backwards use of Bol-Traj. In the "forwards" case `Trajectories.F90` runs on-line with `Bolam.F90`. The result is the position of all particles at each time step of the meteorological model. In the "backwards" case it is not possible to run `Trajectories.F90` with `Bolam.F90` on-line. Instead the run must be played off-line and, therefore, it is necessary to save all meteorological fields created by `Bolam.F90` in an external file which is used as input to `Trajectories.F90` in order to obtain the position of all particles at each time step chosen in the backwards mode. The subroutine that runs on-line with `Bolam.F90` in order to produce the output file that contains all meteorological fields is called `wr_btraj.F90`. To obtain the time inversion, `Trajectories.F90` runs on-line with another main program (`BackTraj.F90`) that reads the output file from `wr_btraj.F90` from the last to the first record, and changes the time sign. Figure 2.2 shows the flow diagram for this case.

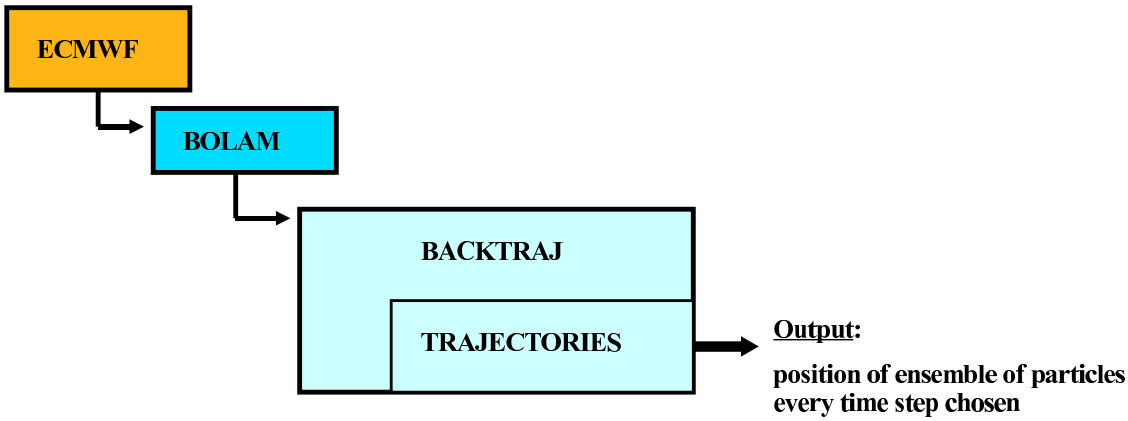

Figure 2.2: flow chart of backward trajectories

A scheme of interaction between the different main codes is summarized below:

- `Bolam.F90` (meteorological code) +`Trajectories.F90` (code of Lagrangian dispersion model)
  + `source.F90` (code for origin of trajectories) + `detection.F90` (code for arrival of trajectories)
  = **Bol-Traj** (forward trajectories)

- `Bolam.F90` (meteorological code) + `wr_btraj.F90` (code saving meteorological fields)
  = **Bol-wr_btraj** (input file for backward trajectories)

- `Back_Trajectories.F90` (Main program for backward trajectories) + `Trajectories.F90` (code of Lagrangian dispersion model)
  + `source.F90` (code for origin of trajectories) + `detection.F90` (code for arrival of trajectories)
  = **Back-Traj** (backward trajectories)

It is important to follow some rules to use the code correctly:

1. input of the model:
   (a) forward trajectories (Bol-Traj)
      i. number of particles
      ii. name of output file
      iii. how many time steps are required between two consecutive outputs
      iv. possibility to choose whether it is necessary to write the output file or not
      v. diffusion coefficient (if it is "zero" the trajectories are deterministic)
   (b) backward trajectories
      - Bol-wr-btraj
        i. name of output file
        ii. how many time steps are required for saving two consecutive meteorological fields
      - Back-Traj
        i. name of input file (the same as output file from Bol-wr-btraj)
        ii. total run time
2. output of the model (output file)
   (a) forward trajectories:
   ASCII format that contains: time step index, trajectory index, longitude (Bolam coordinates), latitude (Bolam coordinates), sigma (Bolam coordinates), velocity (3-components), geographic vertical coordinates (meters)
   (b) backward trajectories:
      - first step: wr-btraj
      binary format that contains: velocity (3 components), geopotential at each point of the 4-dimensional (3-space, 1 time) grid

- second step: backtraj
  ASCII format that contains: time step index, trajectory index, longitude (Bolam coordinates), latitude (Bolam coordinates), sigma (Bolam coordinates), velocity (3-components), geographic vertical coordinates (meters)

3. For each case study it is necessary to write the subroutines of trajectory origin and destination and a file-module to set some variables. Schemes of standard subroutines of aerosol origin and destination and the file-module are given below, showing the obligatory fields to write and set:

   (a) standard subroutine of origin:

   SUBROUTINE source(istep)

   USE mod-traj
   USE mod-source
   USE time-h

   IMPLICIT none

   !arguments
   INTEGER, INTENT(IN) :: istep

   if ((abs(diff-time(source-datetime, sim-datetime))<dtstep).and. (npart-exist==.FALSE.)) then
   call new-coord
   npart-exist=.true.

end if

END SUBROUTINE source

(b) standard subroutine of destination:

SUBROUTINE detection(istep)

IMPLICIT NONE

!arguments
INTEGER :: istep

END SUBROUTINE

(c) standard file-module

MODULE mod-source

USE time-h
USE mod-traj

IMPLICIT none
SAVE

TYPE(tm) ::source-datetime

INTEGER ::source-date,source-time, source-sec

NAMELIST/source-namelist-name/source-date, source-time, source-sec
NAMELIST/detection-namelist-name/'others parameters'

END MODULE mod-source

where:

- *istep* is the time step of the meteorological model,
- *source-datetime* is the date and time of origin of the particles,
- *sim-datetime* is the date and time of start of the simulation,
- *dtstep* is a temporal resolution of the model,
- *npart-exist* is a logical variable that gets the trajectories started
- *new-coord.F90* is a subroutine that transforms the geographic coordinates into model-like coordinates.

2.2.1 Origin of trajectories

An aerosol source must be defined in order to start the dispersion model. Different kinds of aerosol sources exist in nature, such as volcanic eruptions and Saharan dust episodes. For each kind of source a representative scheme has to be developed and a numerical code written. As the origin of trajectories, a non-typical natural source can also be considered, for example, to start trajectories from a measurement instrument (eg. a lidar). In this case, it is necessary to handle it as if it were a natural source, and an adequate scheme must be devised for it. Some examples of appropriate schemes for natural and devised sources of aerosols are given below:

1. a volcano can be represented by a vertical straight line or vertical cylinder with uniform emission, and instantaneous or continuous release in time

2. Saharan dust can be represented by a horizontal surface with non-homogeneous emission in space, and continuous or discrete in time

3. a lidar can be represented by a straight vertical line. The trajectories start from fixed measurement points in space and with instantaneous release in time

2.2.2 Destination of trajectories

Although not necessary for the model, it is sometimes useful for the study to define a destination of the aerosols: for example, when comparing data measured by instruments with model results, or when it is necessary to find out if a trajectory passes a particular point in space. In such cases, a destination scheme must be developed, taking account of the scheme for the origin, since the two schemes must be consistent. If no particular scheme of destination is required, it is sufficient in practice to write a simple subroutine like the example above.

Chapter 3

The experimental measurements

Experimental measurements are an important a tool as the theoretical models, because they provide a "true" reference of reality. They are very useful for comparison with the results of theoretical models, which, instead, do not give real data and can be affected by many errors. A description of the experimental instruments whose measurements are used in this work is given below.

3.1 EARLINET Network - PEARL station

The CNR-IMAA Raman lidar system for tropospheric aerosol study has been operating at Tito Scalo, Potenza (40,63 N, 15,80 E, 760 m asl) since the beginning of EARLINET in May 2000. PEARL (Potenza EARlinet Lidar) is based on a Nd:YAG laser with the second (532 nm) and third (355 nm) harmonics generators. First, second and third harmonic beams are separately expanded and then recombined and simultaneously transmitted into the atmosphere. The radiation backscattered by the atmosphere is collected by a Cassegrain reflecting telescope with a primary mirror of 500 mm diameter and combined focal length of 5 m. Three channels are devoted to detect the radiation backscattered from the atmosphere at the 3 laser wavelengths (1064 nm, 532 nm and 355 nm), and two channels to the

Raman radiation backscattered from the atmospheric N_2 molecules at 607 and 386 nm. An additional Raman channel at 407 nm collects radiation backscatter from the water vapour molecules present in the atmosphere. Finally a cubic polarizing beam splitter allows detection of components of backscattered light polarized perpendicular and parallel to the direction of the linearly polarized transmitted laser beam, giving information on the orientation of the particles in the atmosphere. The spectral selection is provided by means of dichroic mirrors and interferential filters with a bandwidth of 0.5 nm. After spectral selection, each optical signal (i.e. the signal at each wavelength) is further split into two signals of different intensity by means of a beam splitter. Their recombination in the signal pre-processing procedure provides a lidar signal with a good statistic that well describes both the low altitude range, where the backscattered signal is very strong, and the free troposphere region, where the backscattered signal is weak, thus overcoming the detector's limited counting scale interval. The combined Raman/elastic approach furnishes independent measurements of aerosol extinction and backscatter coefficients, and, hence, the lidar ratio at 532 nm and 355 nm. The aerosol backscatter coefficient at 1064 nm is retrieved with an iterative approach starting from the elastically backscattered lidar signal at this wavelength and assuming a lidar ratio profile at 1064 nm. The CNR-IMAA Raman/elastic lidar system allows the determination of aerosol optical properties from the lower troposphere up to the upper free troposphere. For low altitudes, it should be considered that the full overlap between the transmitted laser beam and the telescope field of view is reached at about 0.8 km above the lidar station. Since the determination of the aerosol backscatter coefficient profiles at 355 nm and 532 nm involves the ratio of two lidar signals, these profiles typically start from 400 m above the ground. After a correction for the incomplete overlap, profiles of the aerosol extinction coefficient at 532 nm and 355 nm and of the aerosol backscatter coefficient at 1064 nm typically start from 500 m above the lidar station. Aerosol

optical property vertical profiles are typically obtained with 30 minutes of temporal integration, with a vertical resolution of 60 m for the aerosol backscatter coefficient, and ranging between 60 and 240 m for the aerosol extinction coefficient and lidar ratio. In night time conditions, typical statistical errors due to signal detection are below 5% and 10% in the PBL for the aerosol backscatter coefficients at 355 and 532 nm, and extinction coefficient at 355 nm, respectively. In the free troposphere, typical errors are below 30% for aerosol backscatter at 355 and 532 nm and aerosol extinction, when values of the aerosol extinction are higher than about 5 Mm^{-1}.

3.2 CALIPSO satellite

The CALIPSO payload consists of three co-aligned nadir-viewing instruments:

1. the Cloud-Aerosol Lidar with Orthogonal Polarization (CALIOP) is a two-wavelength polarization-sensitive lidar that provides high-resolution vertical profiles of aerosols and clouds. CALIOP utilizes three receiver channels: one measuring the 1064 nm backscatter intensity, and two measuring orthogonally polarized components of the 532 nm backscattered signal. Dual 14-bit digitizers on each channel provide an effective 22-bit dynamic range. The receiver telescope is 1 meter in diameter. A redundant laser transmitter is included in the payload. The instruments are designed to operate autonomously and continuously, although the data are acquired only under daylight conditions.

2. the Imaging Infrared Radiometer (IIR) is a nadir-viewing, non-scanning imager having a 64 km by 64 km swath with a pixel size of 1 km. The CALIOP beam is nominally aligned with the center of the IIR image. The instrument uses a single microbolometer detecter array, with a rotating filter wheel providing measurements at three channels in the thermal infrared window region at 8.7 mm, 10.5 mm, and 12.0 mm. The wavelengths were

selected to optimize joint CALIOP/IIR retrievals of cirrus cloud emissivity and particle size.

3. the Wide Field Camera (WFC) is a modified version of the commercial off-the-shelf Ball Aerosopace CT-633 star tracker camera. It is a fixed, nadir-viewing imager with a single spectral channel covering the 620-670 nm region, selected to match band 1 of the MODIS (MODerate resolution Imaging Spectroradiometer) instrument on Aqua.

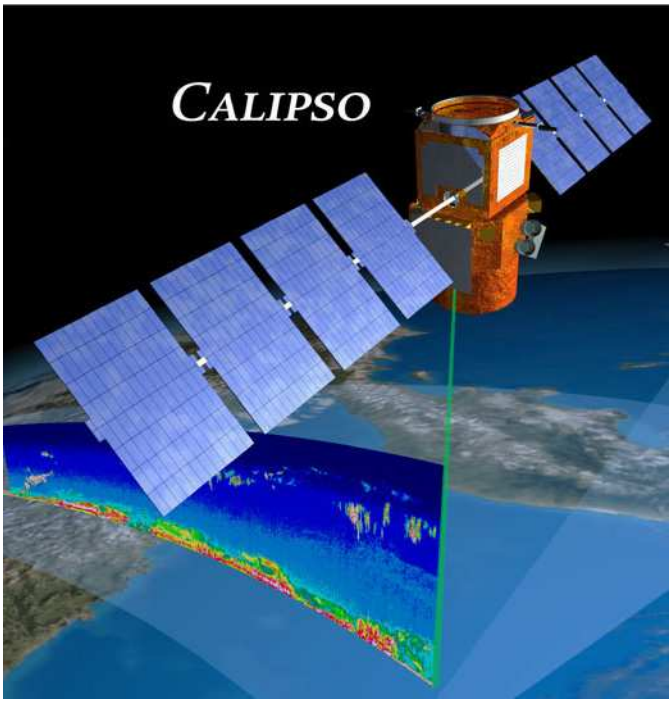

Figure 3.1

3.3 PEARL vs CALIPSO

The comparison between PEARL and CALIPSO measurements is rather complex, being a comparison between spaceborne and ground-based lidars. The attenuated

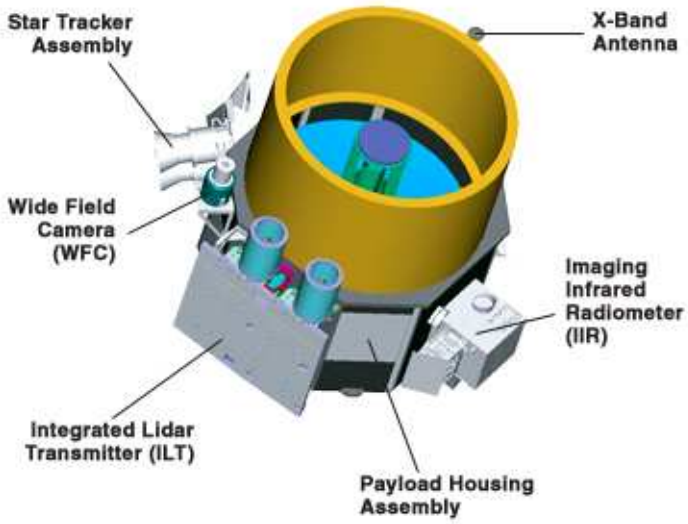

Figure 3.2

backscatter coefficient β' provided by CALIPSO is defined at each altitude z as (18):

$$\beta'(z) = \beta^{Tot}(z)T^2_{par}(z)T^2_{mol}(z)T^2_{O_3}(z) \tag{3.1}$$

where β^{tot} is the backscatter coefficient resulting from particles, molecular and ozone contributions:

$$\beta^{tot}(z) = \beta_{par}(z) + \beta_{mol}(z) + \beta_{O_3}(z) \tag{3.2}$$

and $T^2_{mol}(z)$, $T^2_{O_3}$ and $T^2_{par}(z)$ are the transmission terms present in the elastic lidar equation due, respectively, to the molecules, ozone and particles contained in the atmospheric layer extending between the lidar and the z range. The attenuated backscatter profiles provided by CALIPSO are not directly comparable to PEARL profiles, and a special procedure has been developed for this purpose (18) (17). In retrieving an attenuated backscatter profile from PEARL data, it has to be taken into account that PEARL and CALIPSO transmission terms are different, the former being an upward looking lidar, the latter a downward looking lidar. The

first step is to determine the molecular and ozone terms. The molecular terms in (3.1), both backscatter coefficient and transmission, can be obtained by a co-located radiosounding, if available, or well approximated using a modelled atmosphere. The ozone terms can be estimated starting from ozone profiles available directly as meteorological data embedded in CALIPSO Level 1 products and taking into account the ozone absorption at 532 nm in the Chappuis band. The second step is to calculate the aerosol extinction coefficient and backscatter coefficient for the ground-based lidar, which are retrieved by the conventional Fernald inversion method (31). Using the Fernald technique, two assumptions for aerosol are made. First, it is assumed that the lidar ratio is constant with altitude z (without clouds) and the value is selected. If there is a cloud in the atmosphere, its lidar ratio is calculated using the transmittance method, that is, by first calculating the cirrus cloud optical depth from the transmittance, and then using the determined optical depth as an extra constraint to retrieve the lidar ratio. The second assumption involves selecting the aerosol backscatter ratio R_{min} at the clean altitude z_c, in order to calculate aerosol backscatter. Making these assumptions, solving the lidar equation yields the aerosol backscatter and extinction coefficient profiles. Finally, the third step, a downward attenuated backscatter for the ground-based lidar is constructed. Here z_r is the maximum altitude at which the ground-based lidar can reasonably perform measurements, taking z_r as a reference altitude. From z_r , a downward attenuated backscatter β'_G is constructed. That is

$$\beta'_G(z) = \beta^{tot} e^{-2\int_z^{z_r} \alpha(z')dz'} \tag{3.3}$$

The spaceborne lidar attenuated backscatterβ'_S can be written as

$$\beta'_S(z) = \beta^{tot} e^{-2\int_z^{z_s} \alpha(z')dz'} \tag{3.4}$$

Generally, z_S ranges from 30 to 34 km, whereas z_r is about 20 km. Since few or no aerosols and few molecules are present in the range from z_r to z_S, β'_G approximately equals β'_S. Therefore, β'_G can be used for comparison with β'_S . Such considerations

are valid for comparing measurements from spaceborne and ground-based lidars in elastic configuration. However, at the PEARL station it is also possible to have a configuration that allows independent measurements of particle extinction and aerosol backscatter profiles. In fact, the particle transmission term for a downward looking lidar can be written as a function of the particle extinction:

$$T^2_{par}(z) = e^{-2\int_z^{zs} \alpha_{par}(\zeta)d\zeta} \tag{3.5}$$

where z_s indicates the satellite-borne lidar altitude. Therefore, starting from simultaneous and independent measurements of aerosol backscatter and extinction profiles measured by PEARL, it is possible to calculate the CALIPSO-like attenuated backscatter (CLAB) profile at 532 nm without any assumptions.

3.4 MODIS satellite

MODIS (or Moderate Resolution Imaging Spectroradiometer) is a key instrument onboard the Terra (EOS AM) and Aqua (EOS PM) satellites. Terra's orbit around the Earth is timed so that it passes from north to south across the equator in the morning, while Aqua passes south to north across the equator in the afternoon. Terra MODIS and Aqua MODIS view the entire Earth's surface every one to two days, acquiring data in 36 spectral bands, or groups of wavelengths. These data will improve the understanding of global dynamics and processes occurring on the land, in the oceans, and in the lower atmosphere. MODIS plays a vital role in the development of validated, global, interactive Earth system models able to predict global change accurately enough to assist policy makers in making decisions concerning environmental protection. The MODIS instrument provides high radiometric sensitivity in 36 spectral bands ranging in wavelength from 0.4 microns to 14.4 microns. The responses are customised to the individual needs of the user community and provide exceptionally low out-of-band response. Two bands are imaged at a nominal resolution of 250 m at nadir, with five bands at 500

m, and the remaining 29 bands at 1 km. A 55-degree scanning pattern at the EOS orbit of 705 km achieves a 2330-km swath and provides global coverage every one to two days. The Scan Mirror Assembly uses a continuously rotating double-sided scan mirror to scan 55-degrees and is driven by a motor encoder built to operate at 100 percent duty cycle throughout the 6-year instrument design life. The optical system consists of a two-mirror off-axis afocal telescope, which directs energy to four refractive objective assemblies; one for each of the VIS, NIR, SWIR/MWIR and LWIR spectral regions to cover a total spectral range of 0.4 to 14.4 microns. A high-performance passive radiative cooler provides cooling to 83K for the 20 infrared spectral bands on two HgCdTe Focal Plane Assemblies (FPAs). Novel photodiode-silicon readout technology for the visible and near infrared provides unsurpassed quantum efficiency and low-noise readout with exceptional dynamic range. Analog programmable gain and offset and FPA clock and bias electronics are located near the FPAs in two dedicated electronics modules, the Space-viewing Analog Module (SAM) and the Forward-viewing Analog Module (FAM). A third module, the Main Electronics Module (MEM) provides power, control systems, command and telemetry, and calibration electronics. The system also includes four on-board calibrators as well as a view to space: a Solar Diffuser (SD), a v-groove Blackbody (BB), a Spectroradiometric calibration assembly (SRCA), and a Solar Diffuser Stability Monitor (SDSM). MODIS data, together with all the data from other instruments on the Terra and Aqua satellites, are transferred to ground stations at White Sands, New Mexico, via the Tracking and Data Relay Satellite System (TDRSS). The data are then sent to the EOS Data and Operations System (EDOS) at the Goddard Space Flight Center. The Level 1A, Level 1B, geolocation and cloud mask products and the Higher-level MODIS land and atmosphere products are produced by the MODIS Adaptive Processing System (MODAPS), and are then parceled out among three DAACs for distribution. Ocean color products are produced by the Ocean Color Data Processing System (OCDPS) and distributed

to the science and applications community. The many data products derived from MODIS observations describe features of the land, oceans and atmosphere that can be used to investigate processes and trends on local to global scales.

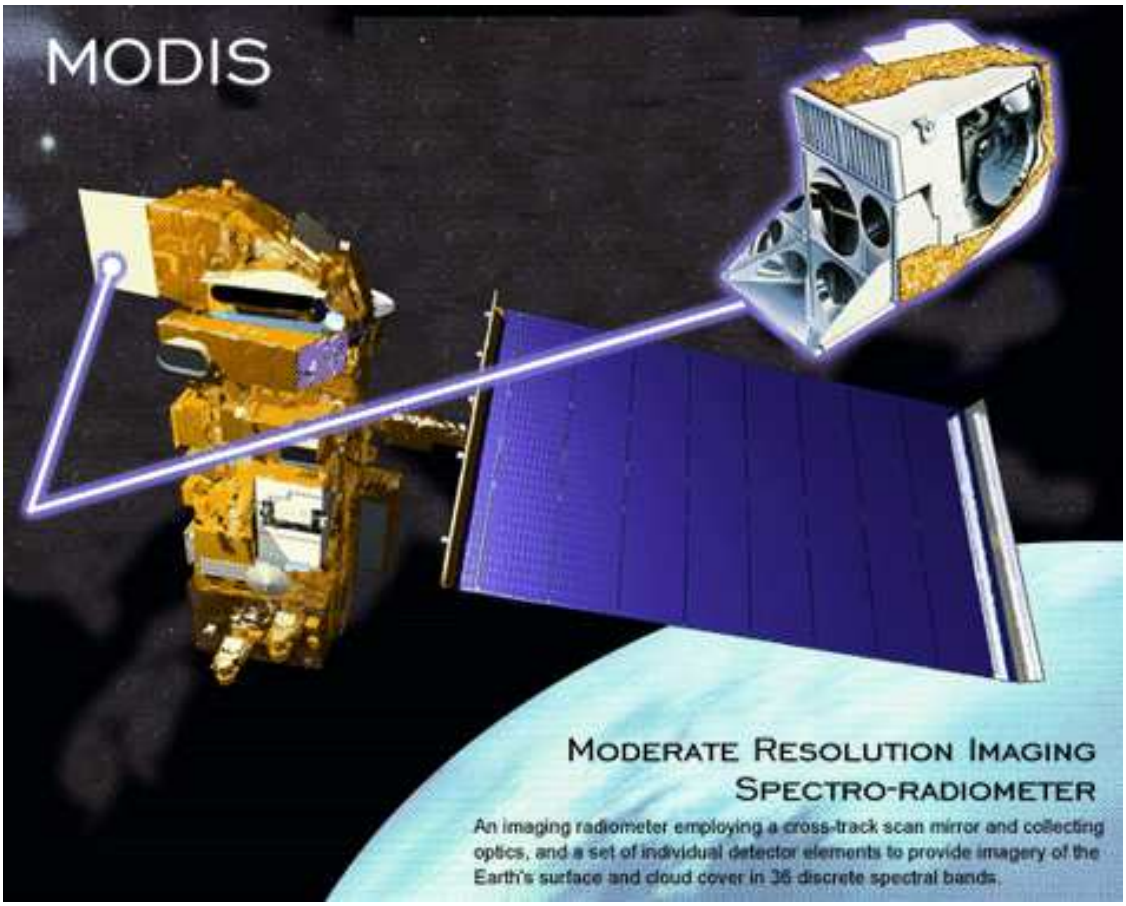

Figure 3.3

Chapter 4

Theoretical model and experimental measurement integration: case studies

The use of theoretical models together with experimental measurements is the best way to study the transport of aerosol in the atmosphere.

Three applications of integration between models and measurements are presented:

1. CALIPSO-PEARL: measurements from space are compared to ground-based measurements using the transport model. The aim is to compare data measured in different space-time references. In this way, it is possible to determine when

   (a) the data is useful for making a direct comparison between the different instruments

   (b) the data is useful for studying the 4-dimensional distribution of aerosol in the atmosphere

Moreover, this integration allows the reconstruction of an aerosol profile at a different space-time point from the point of measurement.

2. ETNA eruption 2002: use of the transport model permits the explanation of experimental measurements. The back-trajectories starting from the measurement points indicate the provenance of the different aerosol layers.

3. Forest Fires - August 2007: the integration between the transport model and different experimental measurements permits the estimation of the plume height of the forest fires.

4.1 Case study: CALIPSO-PEARL

The purpose is to compare the same quantity measured by two different instruments. CALIPSO gives the measurement of a quantity (eg. attenuated backscatter) from space to ground, while PEARL does the same but from ground to space. They also have two different space-time collocations. The methodology is to apply the Bol-Traj model to make a comparison. One of the two instruments is considered the "origin" of particles (start of trajectories) and the other the "destination" of particles (arrival of trajectories), and the particles are transported by the model. The measurement time of CALIPSO is short. It covers a distance of about 500 km in 8 seconds, so 100 profiles at different points are scanned very rapidly. By contrast, the measurement time of PEARL is longer (a few hours), so fewer profiles are available (one every 10 minutes) for a fixed point in space. For the comparison, it is necessary to find the profile within the CALIPSO data that actually arrives over Potenza, transported by the motion of the wind, and to identify the profile within PEARL data so that the measurement time coincides with the arrival time of the CALIPSO profile transported. Because the CALIPSO measurement time is shorter than the time resolution of the model (3 minutes in this case), while the PEARL measurement time is longer, the CALIPSO measurement

is considered instantaneous in time. For this reason CALIPSO is chosen as the origin of the trajectories and PEARL as the destination.

4.1.1 Starting point of aerosols: scheme of source

The portion of the CALIPSO orbit nearest the PEARL station (maximun distance is about 100 km) is considered. Nl is the number of longitudinal and latitudinal points and nh is the number of points in height, so that nl is the total number of profiles of a measured quantity (in this case attenuated backscatter coefficient). The scheme proposed to represent the origin of trajectories is a large grid, where the centre of each cell represents the measurement point. Using the model, the 4 vertices of the cells are displaced. The vertices are the origin of the trajectories. All possible deformations of the grid surface, without gaps, are considered, since the cells are contiguous.

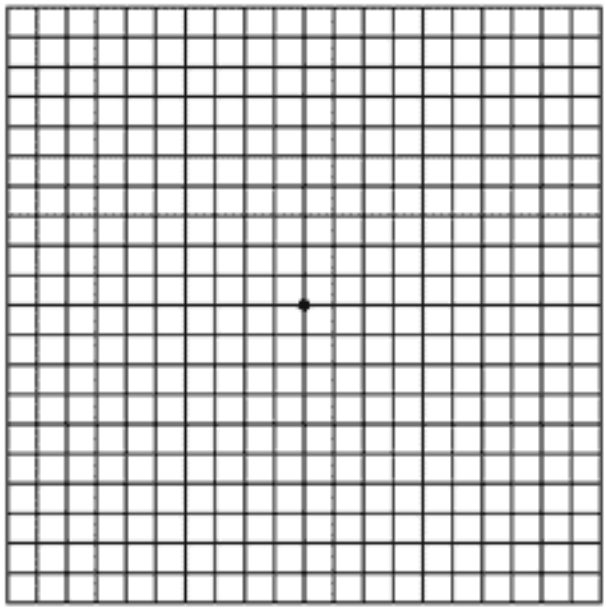

Figure 4.1: case study: CALIPSO-PEARL. Scheme of trajectories origin

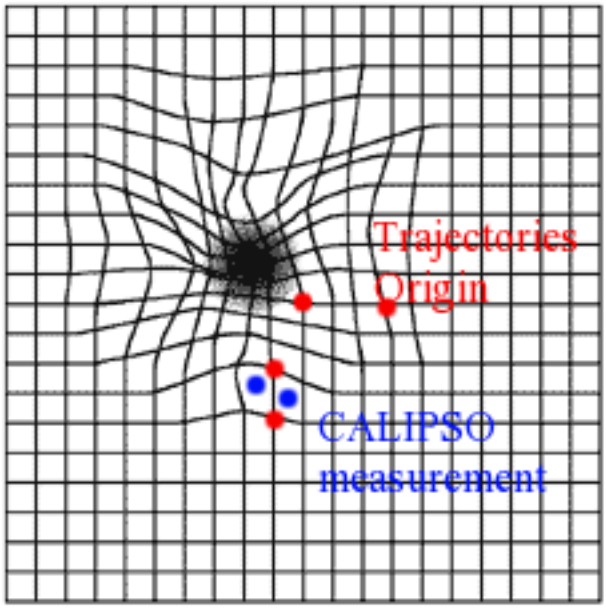

Figure 4.2: case study: CALIPSO-PEARL. Scheme of trajectories origin in movement

4.1.2 End point of aerosols: scheme of detection

The PEARL station gives a vertical scanning of the atmosphere at a fixed longitudinal/latitudinal point. The scheme proposed to represent the lidar measurement profile is a vertical straight line. The aim is to find the intersections between the CALIPSO grid cells and the vertical straight line that represents PEARL. For this purpose all vertices of the CALIPSO grid are displaced and the following algorithm is applied:

1. choose a contour near to PEARL (all vertices of the cells must be within this contour); this reduction of the domain near PEARL allows a decrease in computation cost

2. find the barycentre of the displaced cells

3. compute the 2-dimensional distance (horizontal, longitude/latitude) between the barycentre found and the PEARL station

4. establish the minimum distance variable in time, computed for each cell passing in the lidar domain in each time step. At each time step the values of the distance at current and precedent time steps are stored. When the distance at current time step is bigger than the distance at previous time step then the minimum is found (the minimum distance is in the previous time step).

5. consider the two consecutive surfaces that have a minimum distance and project the 8 points on a horizontal plane (4 vertices of 2 cells); this gives the cells a thickness determined by the space covered in one time step (if the cells does not have a thickness, it is impossible to know when the vertical cell intersects the straight line of the lidar, because the computational time is not continuous)

6. determine the fit that passes between the barycentres of the 2 cells

7. consider the quadrilateral that has 4 of the 8 points as vertices; the choice of points is driven by maximum distance from the fit between the two barycentres; this ensures the maximum surface of projection, thus permitting the greatest probability of intersection

8. check that the projection surface intersects the point (longitude/latitude) representing the PEARL station according to the Jordan Theorem "a point is inside a surface if the half-straight line from this point to infinity intersects an odd number of times the sides of the polygon"

9. if the projection surface intersects the line (i.e. the point is inside the surface), compute the barycentre of the vertical cell that intersects the line and estimate the height

10. write the index of time and index of surface of the CALIPSO grid, and their respective heights in a output file.

4.1.3 Simulations, Analyses and Results

The attenuated backscatter coefficient is chosen as the measurement to be compared between the two instruments, as the profiles of this type of measurement are available from both CALIPSO and PEARL. From PEARL profiles, the attenuated backscatter as observed from the space are calculated as explained in chapter 3.3. Currently, typically comparisons are performed considering the CALIPSO profile nearest PEARL with the PEARL profile measured at the time of overpass of CALIPSO. The newly created method integrates the Bol-Traj model with the experimental measurements, in order to compare the same quantity obtained by different instruments. This tool, theoretically always applicable, imposes certain requirements in order to obtain better results than those achieved with the standard comparison:

1. the scale of the motion of wind must be comparable or less than the distance between two instruments. As shown below, in the case of 25 August 2007, for example, an anticyclonic structure is present over Potenza, providing a very interesting opportunity for study using the new method. Conversely, there is no particular reason to employ it in the case of 22 June 2007, when the wind is direct from CALIPSO to PEARL, so that the nearest profile is very close, and therefore very similar to the transported one.

2. the distance between the two different profiles is comparable, or bigger than the scale of variability of the data measured by CALIPSO. Among 100 profiles scanned by CALIPSO, there can be a large signal variability. The figures 4.11, 4.12, 4.17, 4.18 and 4.19 plot the mean value, mean value plus standard deviation, and mean value minus standard deviation for a chosen level in altitude, along with the values of attenuated backscatter of all the available profiles of CALIPSO. Some cases show no significant signal variability. The others reveal a signal modulation, it being important, however, that the 2 CALIPSO profiles (the nearest and the transported) are in separate regions of the scale of signal variability.

If such requirements are respected, the integration methodology can provide the best results. Since the present work considers both methods, for each case study the root mean square errors are computed, between the PEARL profile and both CALIPSO profiles (the nearest and the transported). In reality, the integration method demands the PEARL profile measured at the times of arrival of trajectories from CALIPSO to PEARL. Unfortunately, however, these data profiles are unavailable, because although PEARL measurements in coincidence with CALIPSO overpassed last typically 3 hours, this long lasting time interval is often not sufficient for obtaining profiles at the times of arrival of trajectories from CALIPSO. The only exception is the case study of 13 August 2007, for which the time shifted PEARL profiles were obtained.

Case:26 June 2006

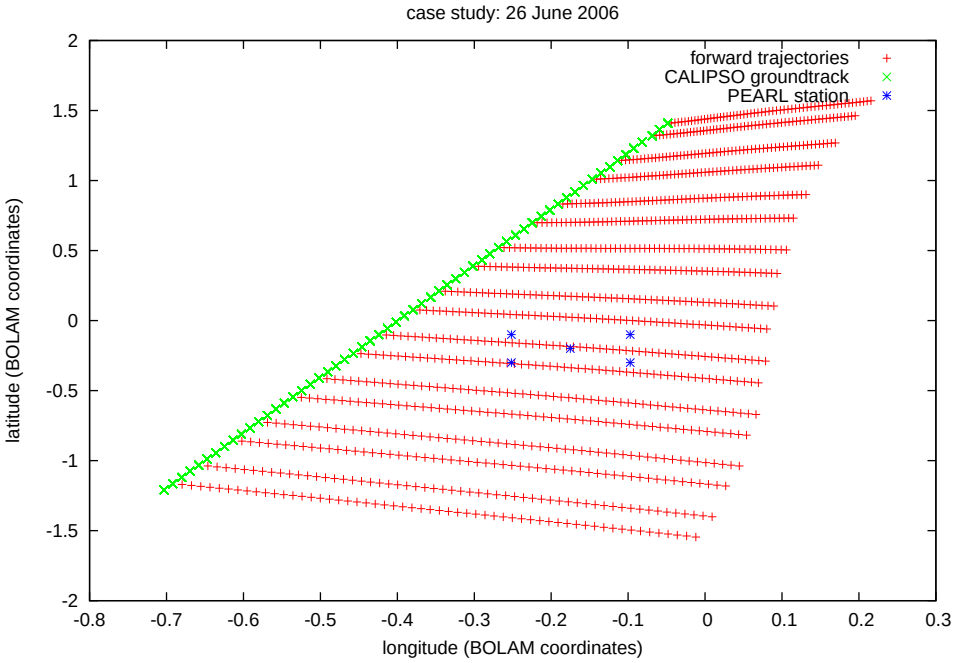

Figure 4.3: Case study: CALIPSO-PEARL 26 June 2006. Forward trajectories from CALIPSO groundtrack to PEARL station

This is a case of wind coming from the north-west. The Bol-Traj model is used in forward mode, because the CALIPSO groundtrack is at north-west with respect to the PEARL station as shown in figure 4.3. The trajectories start from a CALIPSO grid composed of 59 profiles, one every 5 km longitude/latitude and at 3 different vertical resolutions: 30 meters in the range [1017-8182], 37.5 meters in the range [8182-8257] and 60 meters in the range [8257-12034]. Meteorological data are available at the grid points every 20 km, and every 180 seconds. The figure 4.6 plots the difference between CALIPSO profiles (the nearest is number 28, and the transported one is centered on 34), and PEARL profile of attenuated backscatter, measured and averaged from 00:50 to 01:30 with vertical resolution of 60 meters, while the figure 4.4 show the attenuated beackscatter profiles. The

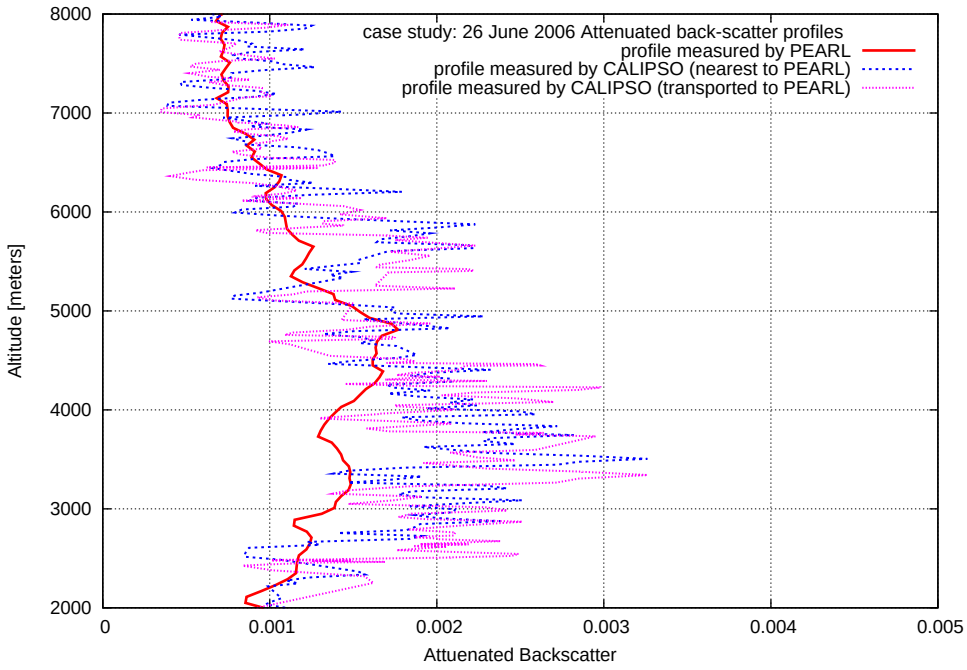

Figure 4.4: Case study: CALIPSO-PEARL 26 June 2006. Attenuated backscatter profiles of CALIPSO nearest to PEARL, CALIPSO transported to PEARL and PEARL measured at overpass time of CALIPSO at 532 nm

root mean square error computed between 2000 and 8000 meters of height of the nearest profile is 5.3 *10(-4), while it is 5.8 *10(-4) for the transported profile. This result does not constitute an improvement on the older method, but, as mentioned above, the time of measurement of PEARL is contemporary with the overpass of CALIPSO. In the figure 4.5, the arrival times of trajectories from the CALIPSO grid to the PEARL station change with the height, with a range of [40-220] minutes after the overpass.

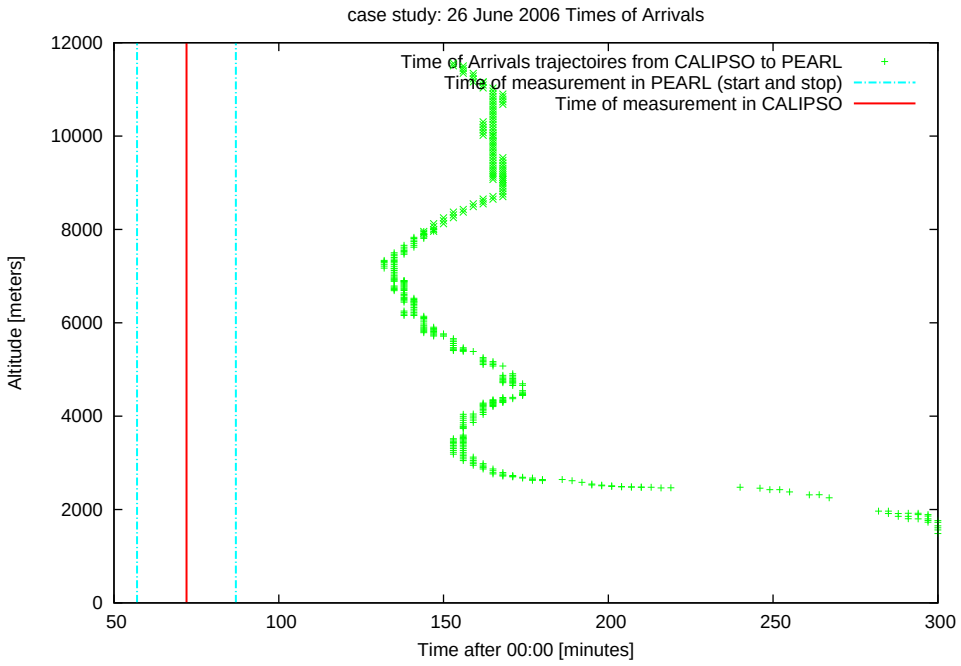

Figure 4.5: Case study: CALIPSO-PEARL 26 June 2006. Arrival times of trajectories from CALIPSO to PEARL

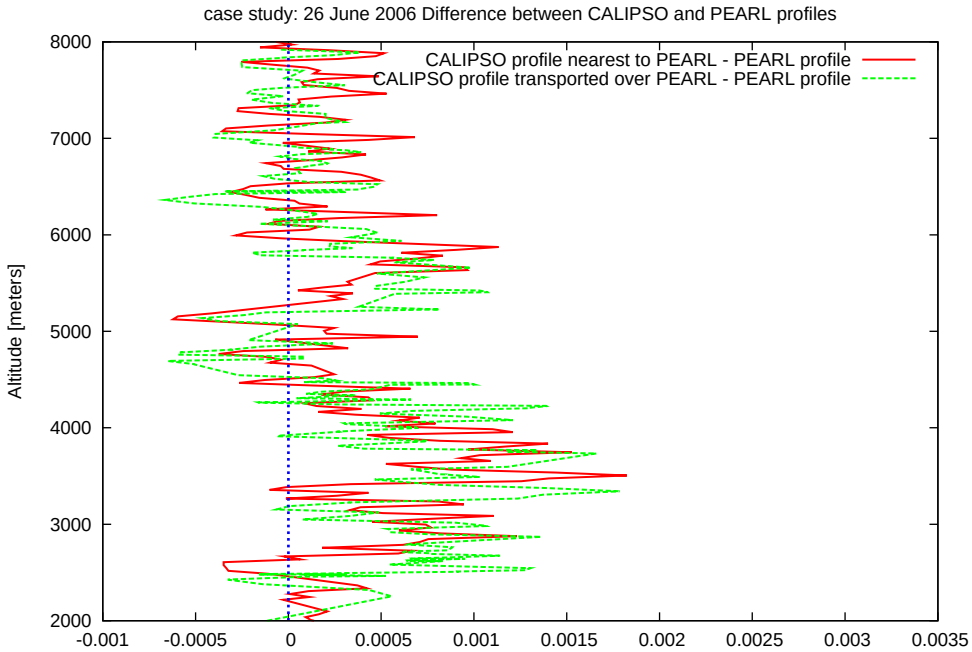

Figure 4.6: Case study: CALIPSO-PEARL 26 June 2006. Difference between CALIPSO transported and CALIPSO nearest profiles and PEARL profile

Case:28 April 2008

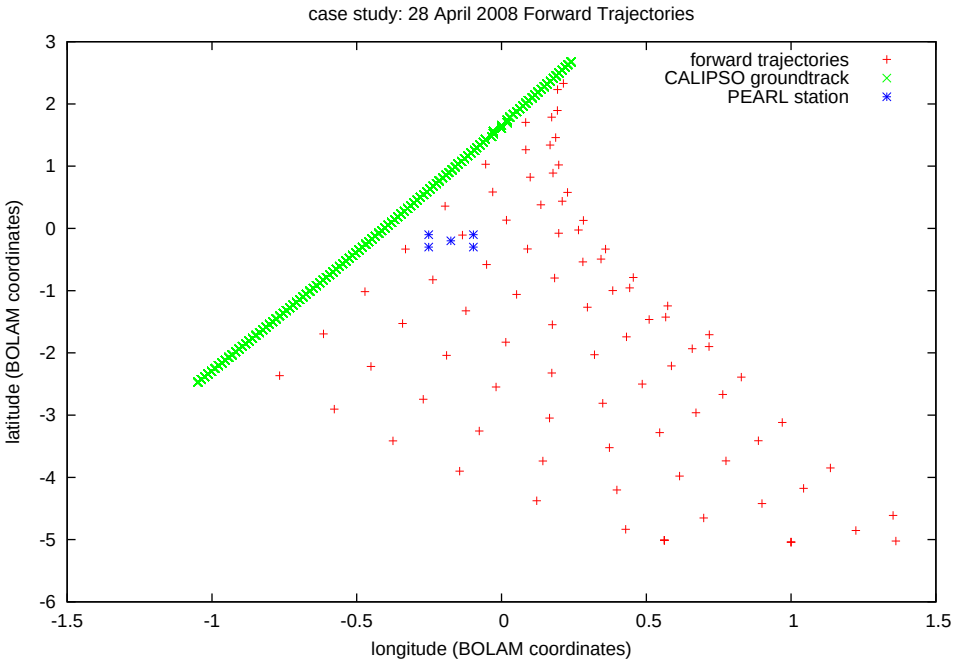

Figure 4.7: Case study: CALIPSO-PEARL 28 April 2008. Forward trajectories from CALIPSO groundtrack to PEARL station

This is a case of wind coming from the north-west. The Bol-Traj model is used in forward mode because the CALIPSO groundtrack is north-west with respect to the PEARL station as shown in figure 4.7. The trajectories start in forward mode at 1:10 34 sec a.m. from a CALIPSO grid that has 116 profiles, every 5 km longitude/latitude, and 3 different vertical resolutions: 30 meters in the range [1017-8182], 37.5 meters in the range [8182-8257] and 60 meters in the range [8257-12034]. Meteorological data are available at the grid points every 20 km, and every 180 seconds. The arrival times of trajectories are very long (400-600 minutes after the PEARL measurement) as shown in figure 4.9 and the distance between two CALIPSO profiles (nearest number 56, transported centered on number 40) is less than the variability of the CALIPSO data signal, as shown in figures 4.11 and 4.12,

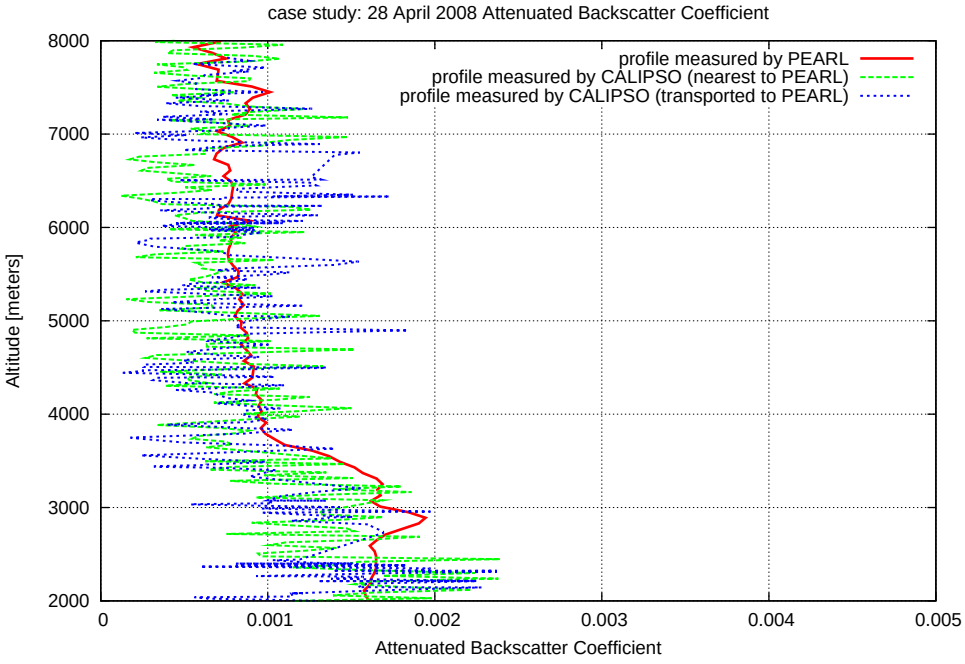

Figure 4.8: Case study: CALIPSO-PEARL 28 April 2008. Attenuated backscatter profiles of CALIPSO nearest to PEARL, CALIPSO transported to PEARL and PEARL measured at overpass time of CALIPSO at 532 nm

where the values of attenuated backscatter coefficient of all profiles are plotted with mean value+ standard deviation and mean value - standard deviation. Therefore, the integration methodology is not found to give a better result than the older one, as is confirmed by the computation of the root mean square errors: 3.8 * 10(-4) for nearest profile and 4.5 *10(-4). Figures 4.11 and 4.12 are related to two different altitudes of the profiles: 2807 meters and 3795 meters. The altitudes were chosen according to specific criteria: the first is a peak of the curve of the attenuated backscatter profile, i.e. a layer with a strong presence of aerosol, as shown in figure 4.8; the second is a layer where the CALIPSO profiles are quite different from the PEARL profile, as shown in figure 4.10.

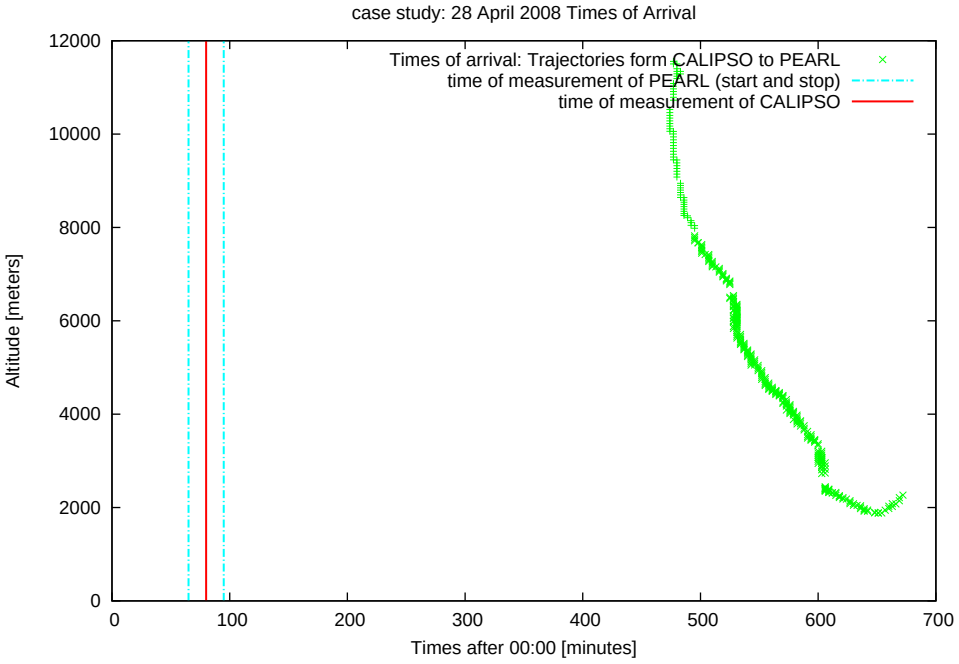

Figure 4.9: Case study: CALIPSO-PEARL 28 April 2006. Arrival times of trajectories from CALIPSO to PEARL

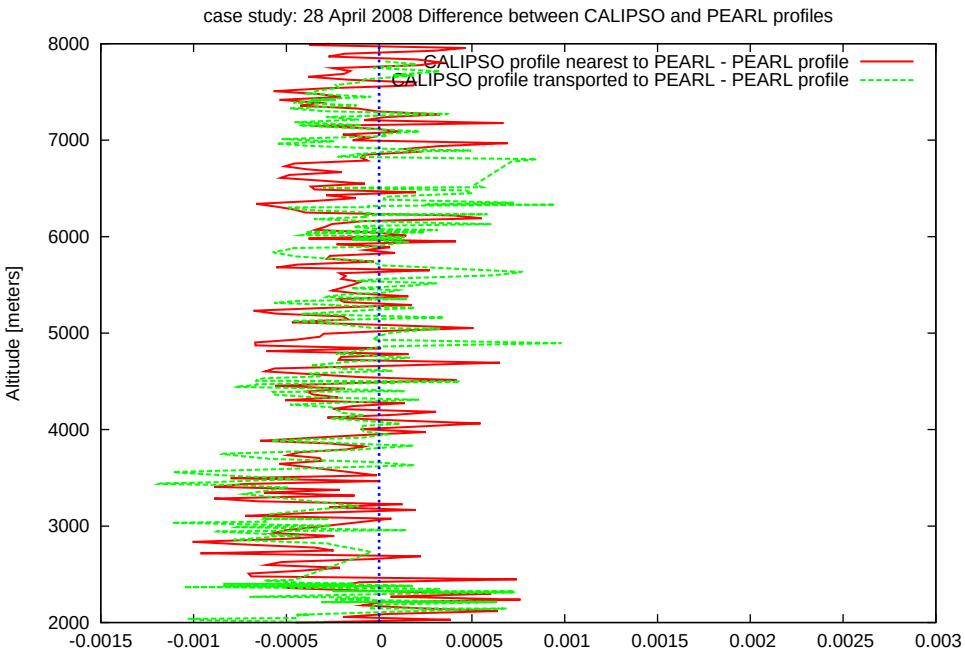

Figure 4.10: Case study: CALIPSO-PEARL 28 April 2008. Difference between CALIPSO transported and CALIPSO nearest profiles and PEARL profile

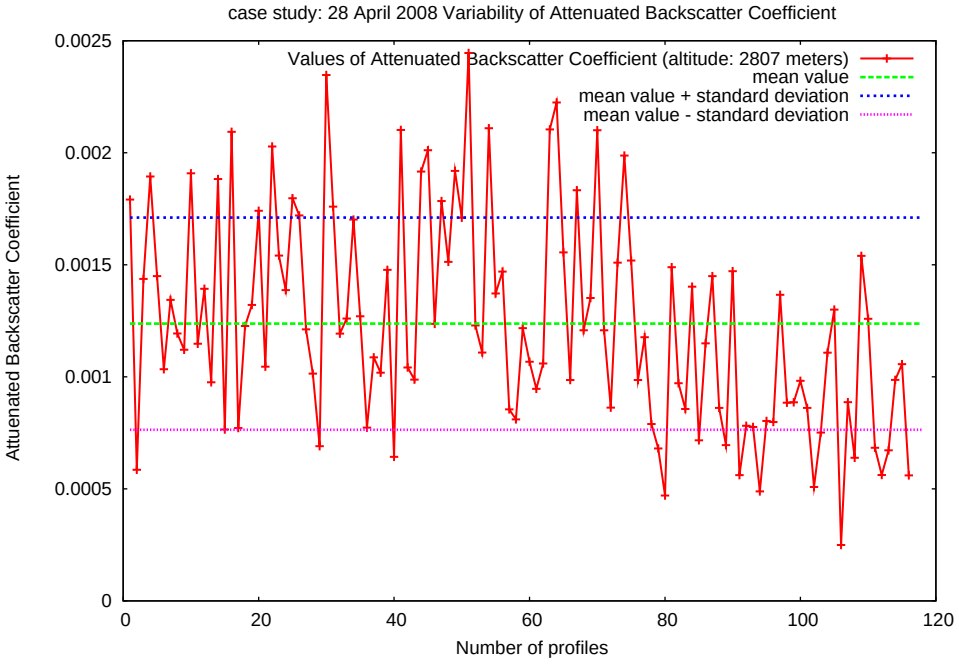

Figure 4.11: Case study: CALIPSO-PEARL 28 April 2008. Mean value, mean value + standard deviation, mean value - standard deviation and attenuated backscatter values at 2807 metres

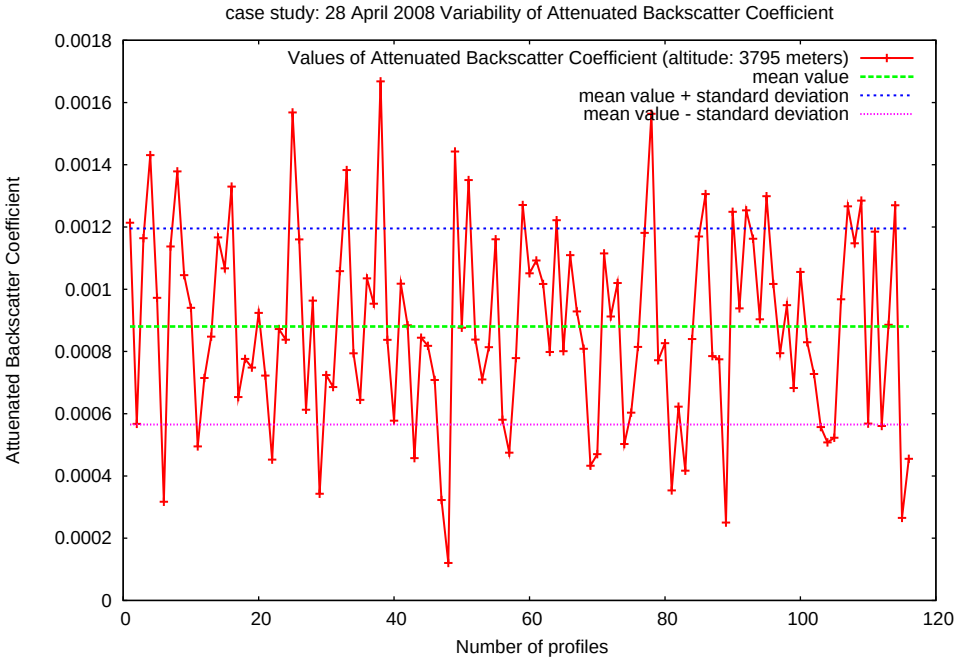

Figure 4.12: Case study: CALIPSO-PEARL 28 April 2008. Mean value, mean value + standard deviation, mean value - standard deviation and attenuated backscatter values at 3795 metres

Case:22 June 2007

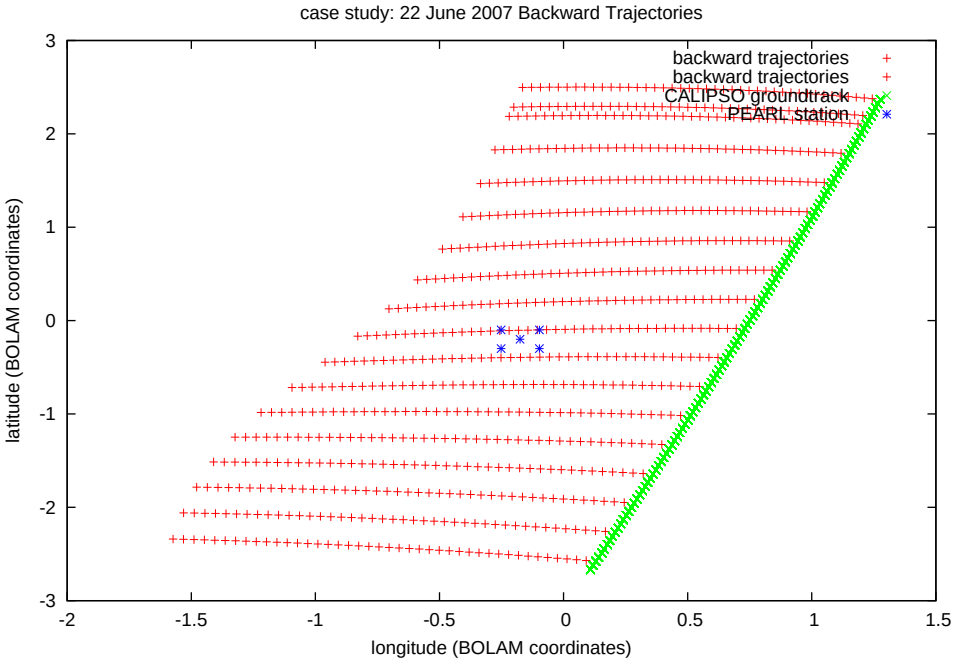

Figure 4.13: Case study: CALIPSO-PEARL 22 June 2007. Forward trajectories from CALIPSO groundtrack to PEARL station

This is a case of wind coming from the north-west. The Bol-Traj model is used in backward mode, because the CALIPSO groundtrack is south-east with respect to the PEARL station as shown in fugure 4.13. The trajectories start at 1:04 and 48 sec a.m. (CALIPSO measurement time) from a grid that has 113 profiles, one every 5 km longitude/latitude and at 3 different vertical resolutions: 30 meters in the range [1017-8182], 37.5 meters in the range [8182-8257] and 60 meters in the range [8257-12034]. Meteorological data are available at the grid points every 20 km, and every 180 seconds, because the wind fields are saved for each time step. The arrival times of trajectories are quite long (120-180 minutes after PEARL measurement), as shown in figure 4.15, and the signal variability at the chosen three levels (6503, 5514 and 3715) reveals a pronounced modulation as shown in 4.19, 4.18 and 4.17.

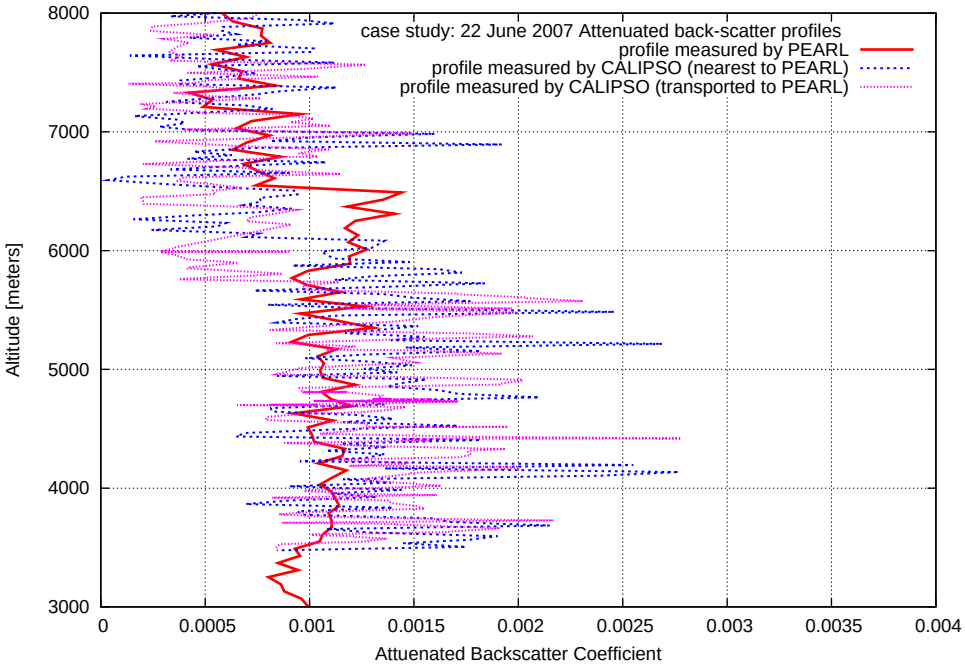

Figure 4.14: Case study: CALIPSO-PEARL 22 June 2007. Attenuated backscatter profiles of CALIPSO nearest to PEARL, CALIPSO transported to PEARL and PEARL measured at overpass time of CALIPSO at 532 nm

Unfortunately, despite this fact, the nearest profile is very close to the transported one (number 59 and 60), so that the distancstance between them is not bigger than the scale of variability. The two root mean square errors computed are 5.0 *10(-4) for nearest and 4.9 * 10(-4) for transported profiles.

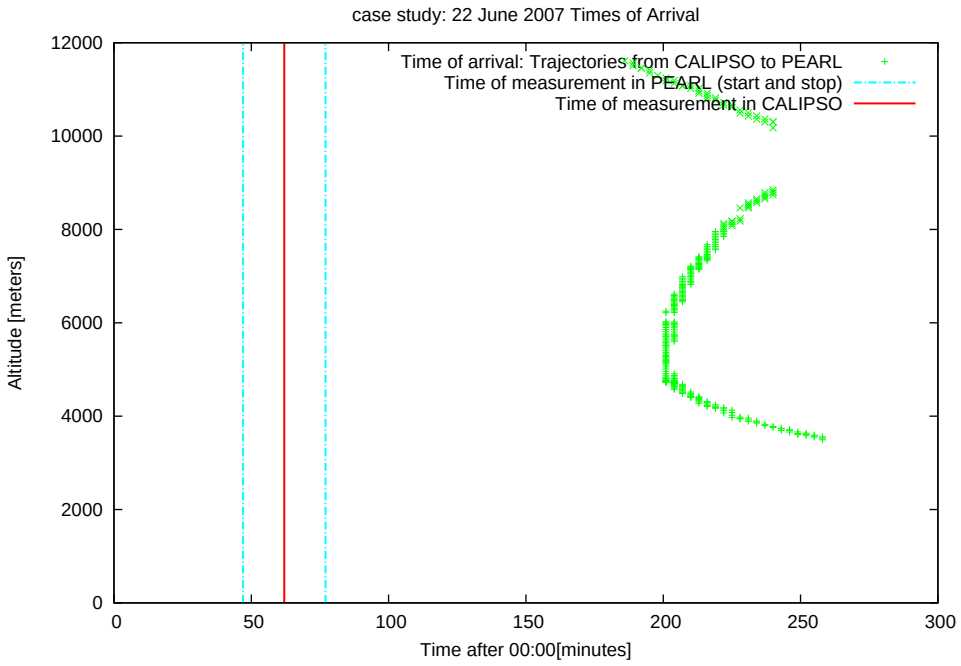

Figure 4.15: Case study: CALIPSO-PEARL 22 June 2007. Arrival times of trajectories from CALIPSO to PEARL

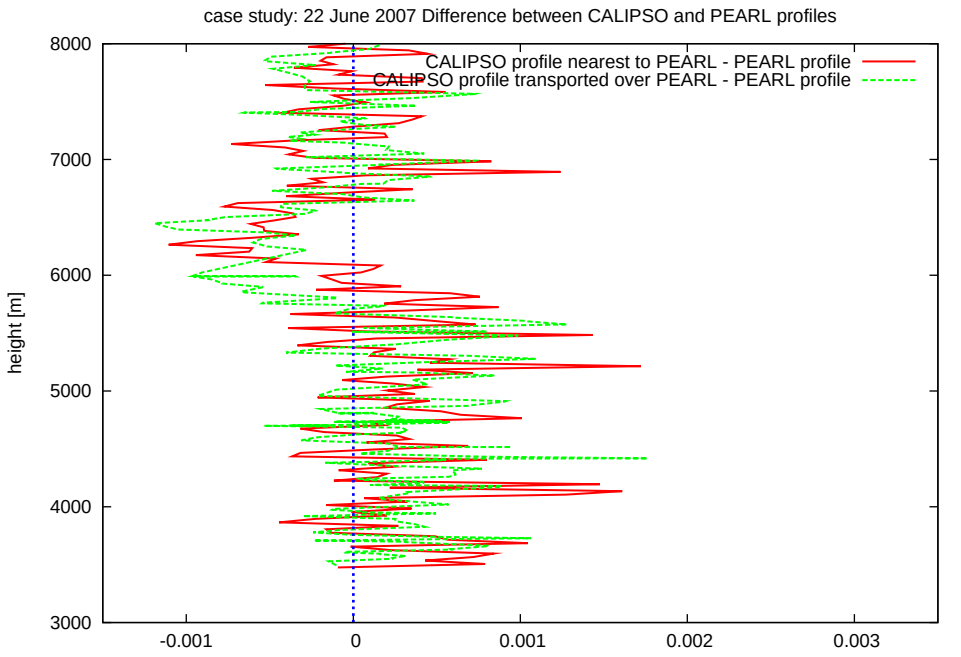

Figure 4.16: Case study: CALIPSO-PEARL 22 June 2007 Difference between CALIPSO transported and CALIPSO nearest profiles and PEARL profile

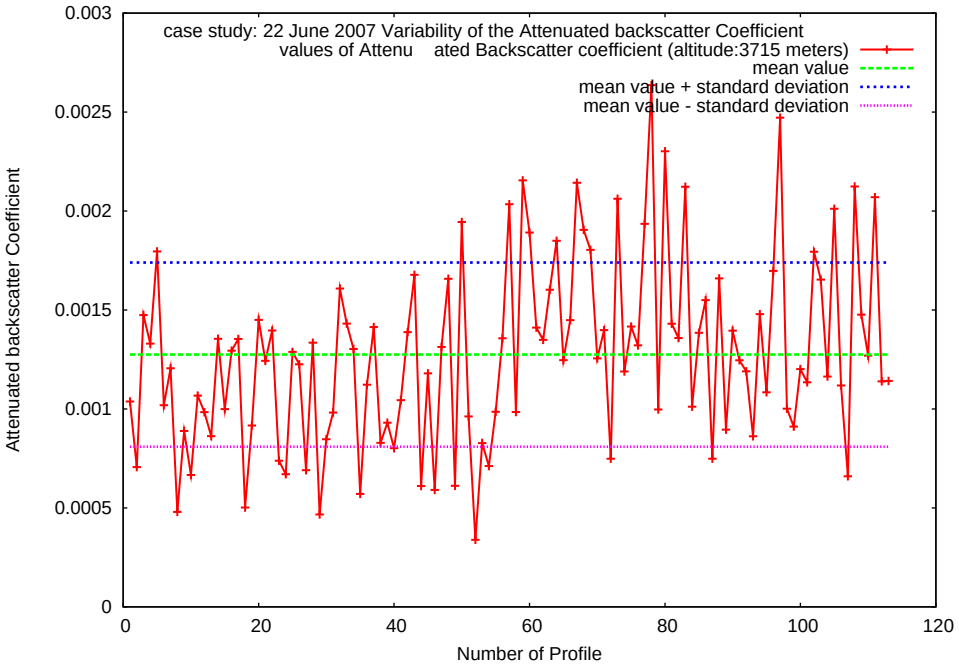

Figure 4.17: Case study: CALIPSO-PEARL 22 June 2007. Mean value, mean value + standard deviation, mean value - standard deviation and attenuated backscatter values at 3715 metres

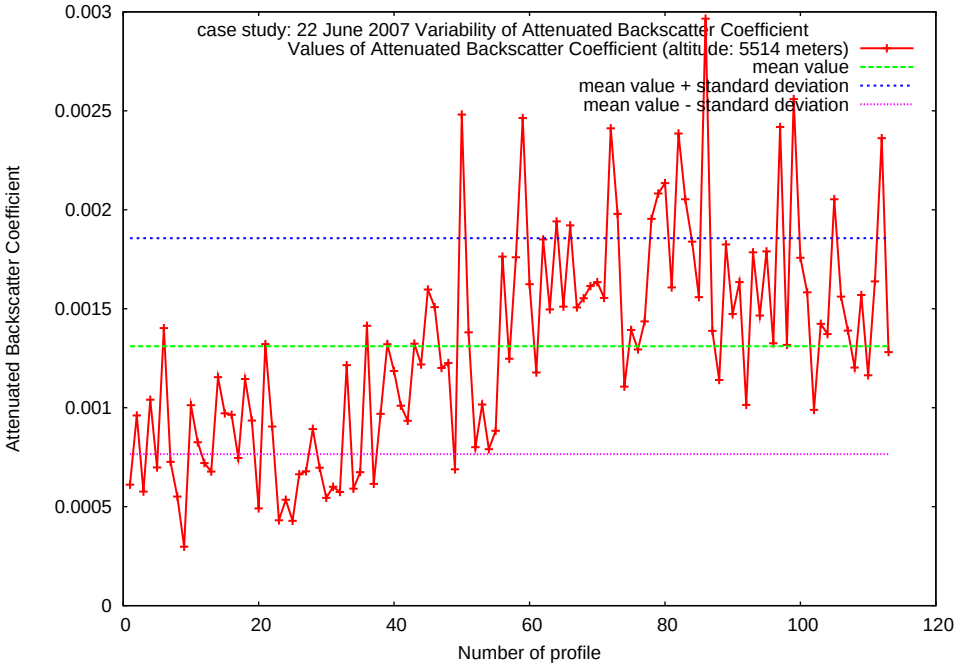

Figure 4.18: Case study: CALIPSO-PEARL 22 June 2007. Mean value, mean value + standard deviation, mean value - standard deviation and attenuated backscatter values at 5514 metres

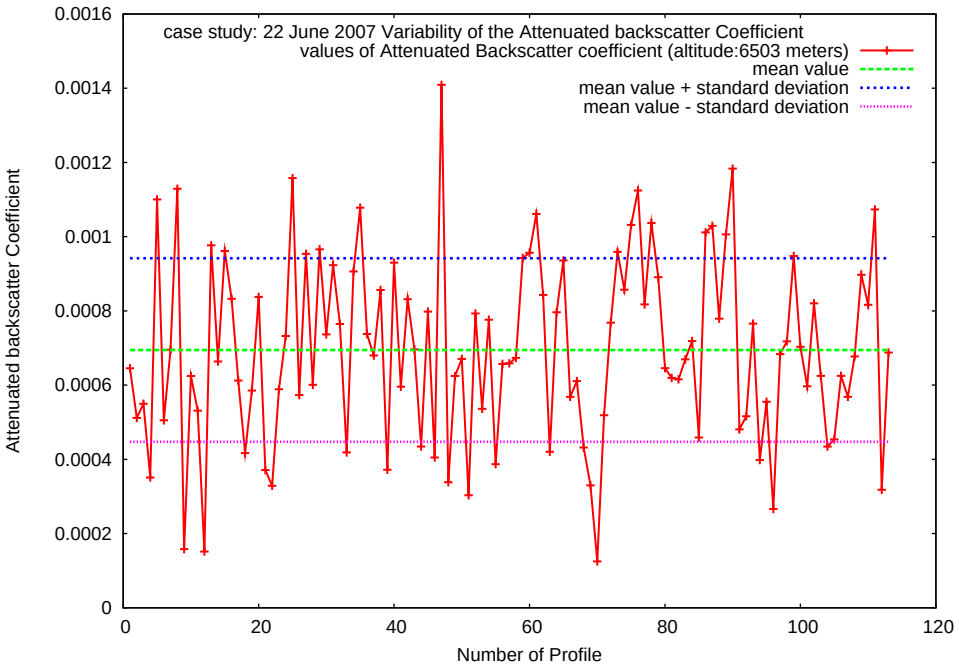

Figure 4.19: Case study: CALIPSO-PEARL 22 June 2007. Mean value, mean value + standard deviation, mean value - standard deviation and attenuated backscatter values at 6503 metres

Case:25 August 2007

The 25 August 2007 is an interesting case study because there is an anticyclonic structure of the wind. The groundtrack of CALIPSO is north-west with respect to Potenza, and it is necessary to make two different simulations, one forward and the other backward, as the wind changes direction with altitude: it is south-easterly over 7000 meters and north-westerly below this height. There is also a circular structure that highlights the presence of an anticyclonic structure. Consequently, the times of arrival of trajectories are very long (figure 4.20), especially at low altitudes, where the trajectories must follow the anticyclonic shape before arriving over Potenza.

The trajectories start at time 1:04 and 48 seconds from the CALIPSO grid, which has 113 profiles in longitudinal/latitudinal points, and vertical resolutions of 30 meters between 2000 and 8000 meters altitude and 60 meters in the 8000-12000 meter range. The meteorological fields are available at every time step of the model (i.e. 180 sec) in forward mode, and every 20 time steps (i.e. 1 h) in backward mode. Figures 4.21, 4.22 and 4.23 show a horizontal projection of the trajectories. The first two figures show the plots of backward and forward trajectories, respectively, between 2000 and 8000 meters, while the third shows the plot of forward trajectories over 8000 meters. In all three figures, the anticyclone structure is quite visible. Unfortunately, at the moment the PEARL data are still not available so that it is impossible to make a comparison with CALIPSO profiles.

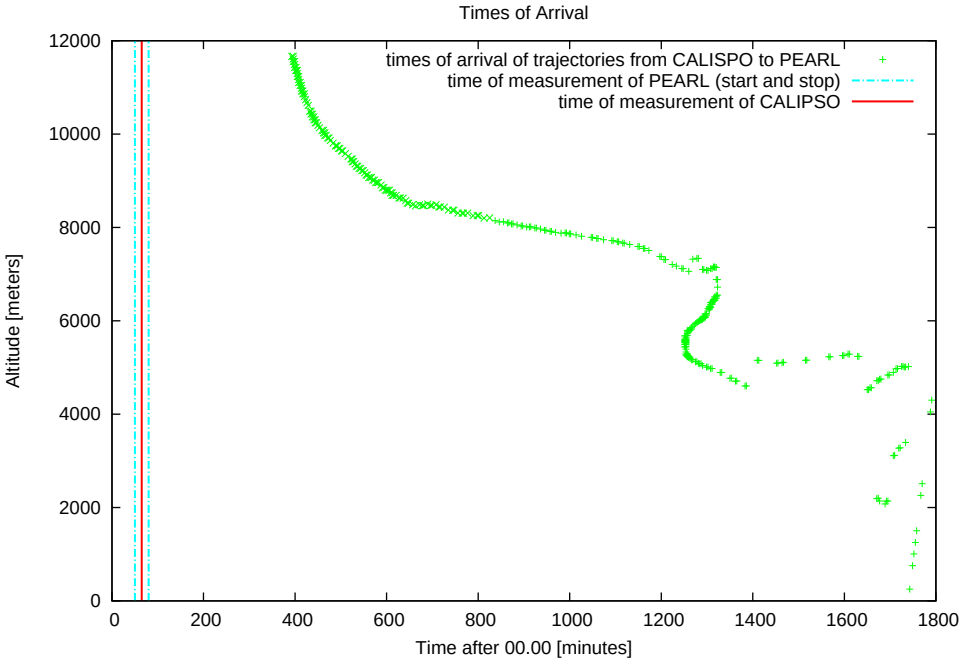

Figure 4.20: Case study: CALIPSO-PEARL 25 August 2007. Arrival times of trajectories from CALIPSO to PEARL

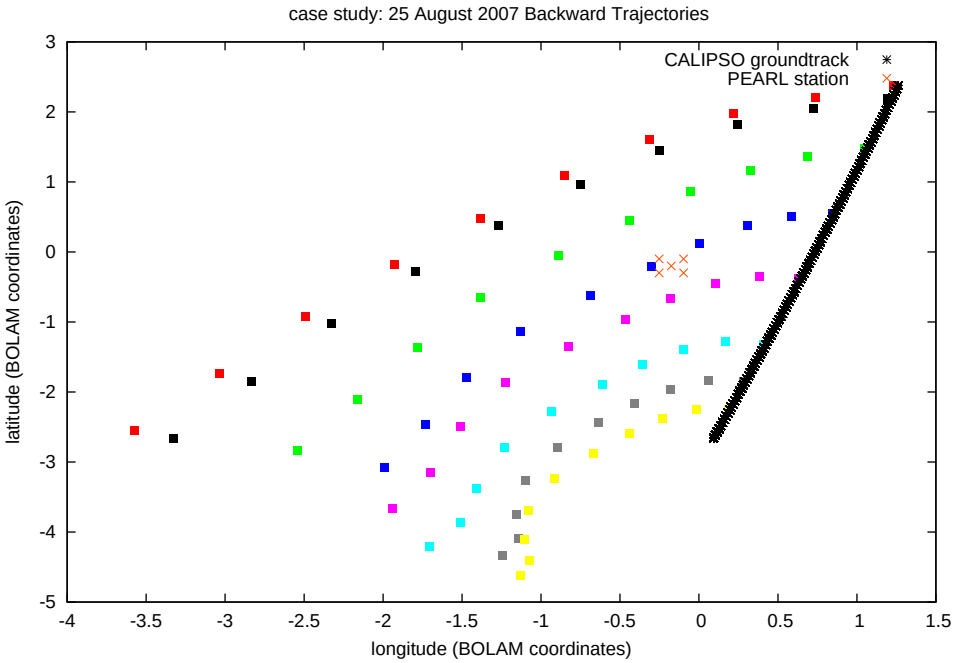

Figure 4.21: Case study: CALIPSO-PEARL 25 August 2007. Backward trajectories from CALIPSO groundtrack to PEARL station between 2000 - 8000 meters

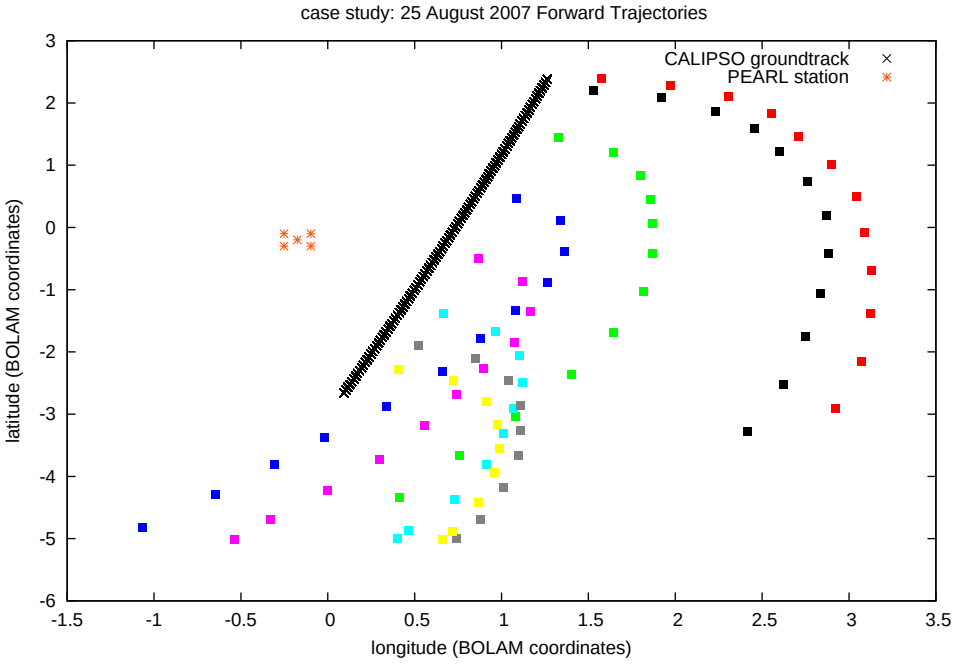

Figure 4.22: Case study: CALIPSO-PEARL 25 August 2007. Forward trajectories from CALIPSO groundtrack to PEARL station between 2000 - 8000 meters

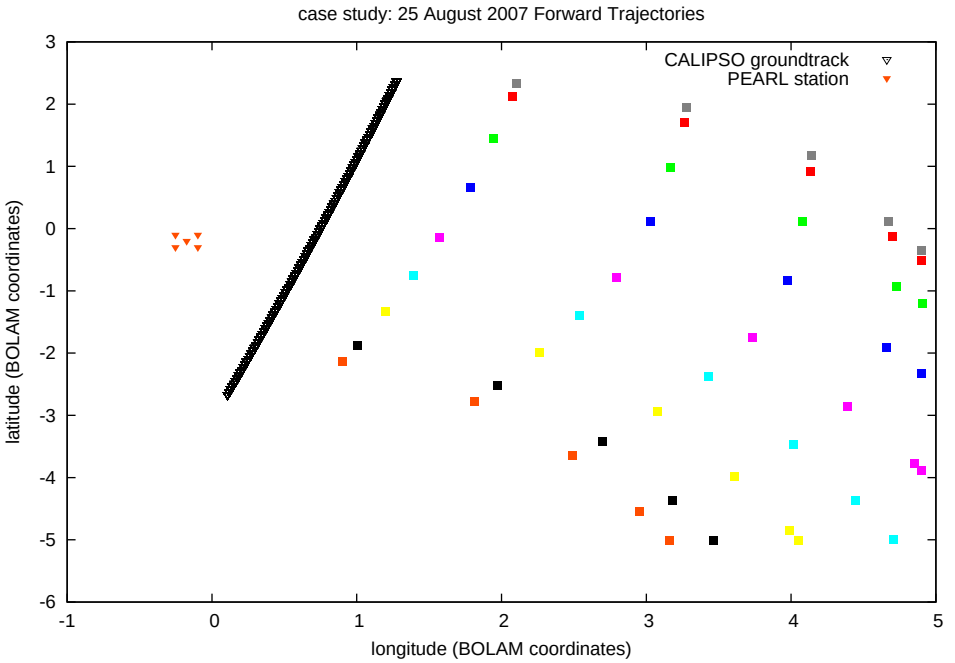

Figure 4.23: Case study: CALIPSO-PEARL 25 August 2007. Forward trajectories from CALIPSO groundtrack to PEARL station over 8000 meters

Case:13 August 2006

The case of 13 August 2007 is worthy of study, because data displaced by a few hours with respect to the CALIPSO overpass time is available in Potenza. The wind is north-easterly and the groundtrack is north-west of Potenza (figure 4.24), so that the forward simulation has been run. The trajectories start at 1:10 and 27 seconds from the CALIPSO grid points: the grid is composed of 118 vertical profiles (i.e. 118 horizontal points), each 5 km and 208 vertical points with resolution of 30 meters in then 1000-8000 meter altitude range, 2 points with resolution 45 meters in the 8000-9000 range, and 64 points with resolution 60 meters over 9000. Figure 4.26 shows the arrival times, which are quite short, with a range of [20-60] minutes after the PEARL measurement. As shown in figure 4.25 the CALIPSO transported profile (blue dashed line) is more similar to PEARL shifted profile (pink dashed line) to respect the others. This fact is confirmed by the computation of root mean square errors, that are computed in four case and the results are listed below:

- CALIPSO nearest to PEARL - PEARL measured at the overpass of CALIPSO $= 4.6 \exp -4$
- CALIPSO transported over PEARL - PEARL measured at the overpass of CALIPSO $= 4.6 \exp -4$
- CALIPSO nearest to PEARL - PEARL measured at arrival times of the trajectories from CALIPSO at PEARL $= 4.6 \exp -4$
- CALIPSO transported to PEARL - PEARL measured at arrival times of trajectories from CALIPSO at PEARL $= 4.0 \exp -4$

Unfortunately, this is the only case in which measurements are available at "true" time. However, these preliminary results suggest that the new methodology is a useful tool for making a comparison between groundbased and satellite

measurements, and for the reconstruction an aerosol profile in a different space-time point with respect to the one of measurement.

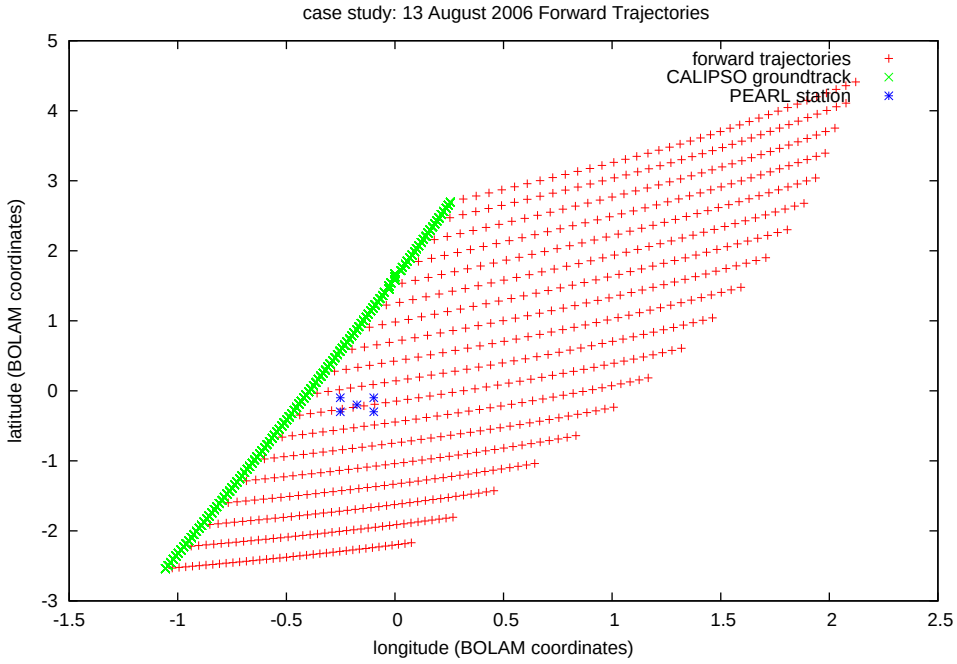

Figure 4.24: Case study: CALIPSO-PEARL 13 August 2006. Forward trajectories from CALIPSO groundtrack to PEARL station

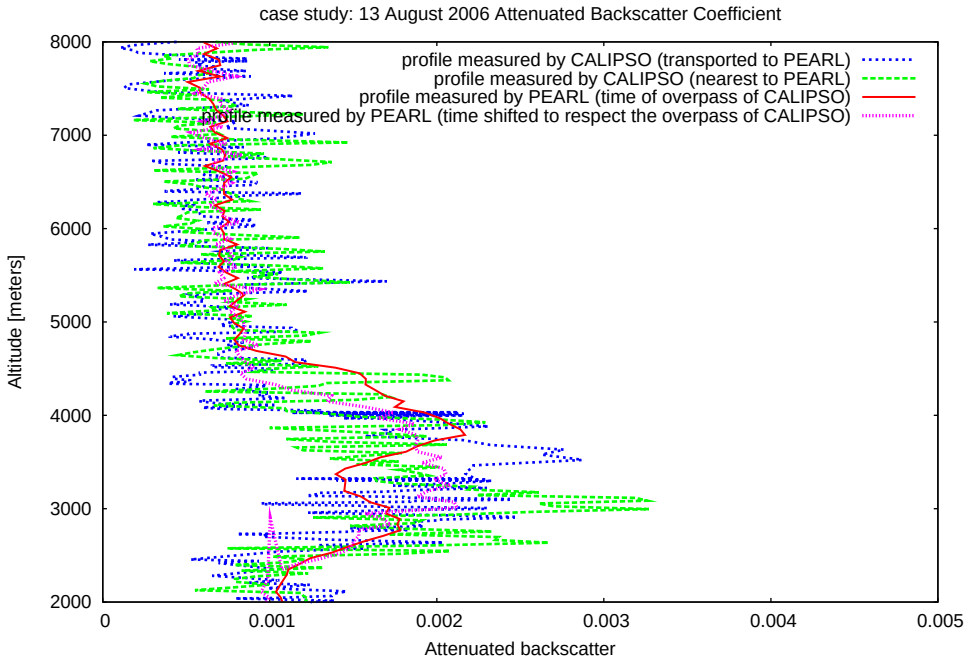

Figure 4.25: Case study: CALIPSO-PEARL 13 August 2006. Attenuated backscatter profiles of CALIPSO nearest to PEARL, CALIPSO transported to PEARL and PEARL measured at overpass time of CALIPSO at 532 nm

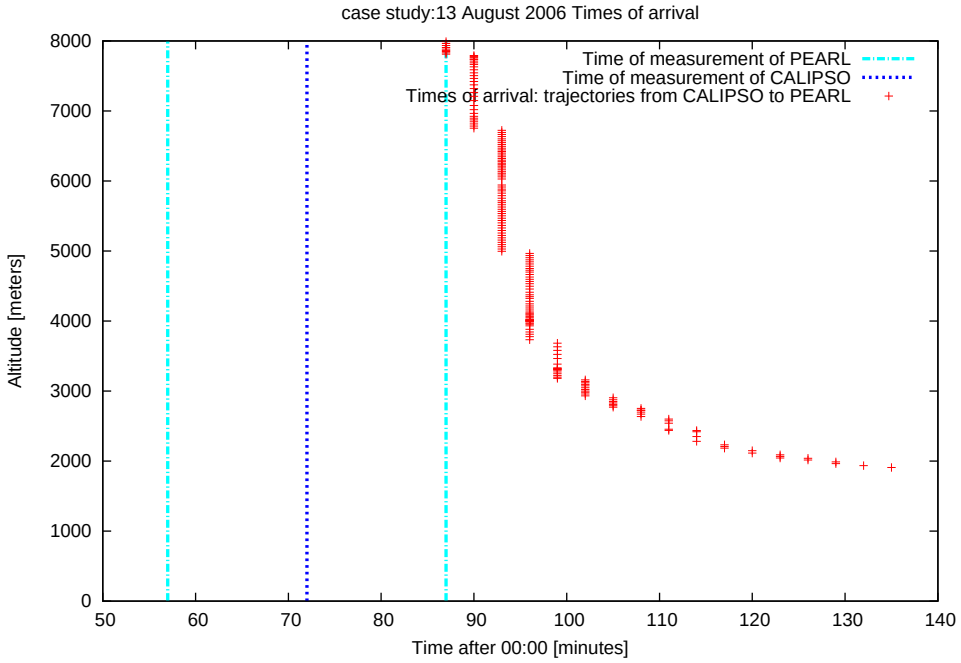

Figure 4.26: Case study: CALIPSO-PEARL 13 August 2006. Arrival times of trajectories from CALIPSO to PEARL

4.1.4 Summary of results

The method based on the integration of the Bol-Traj model with PEARL and CALIPSO experimental measurements is applied to different case studies in order to obtain a comparison between satellite and ground-based data. At present, a method providing a direct comparison between the two types of observation is the state of the art of what can be obtained. For this reason, the results of the integration method are compared with those achieved with the previous one. The standard comparison compares the CALIPSO profile nearest to the PEARL station with the PEARL profile measured at the overpass time of CALIPSO near to PEARL, while the new method compares the CALIPSO profile transported by the Bol-Traj model over Potenza with the PEARL profile measured at arrival times of the CALIPSO profile over Potenza. In order to achieve the best results using the new method, two requirements must be met:

1. the distance between the two instruments must be longer than, or comparable to, the scale of the motion of wind

2. the distance of the signal between the two CALIPSO profiles (nearest and transported) must be longer than, or comparable to, the scale of variability of the CALIPSO profile signal.

Even if in some cases the results obtained using integration method turned out to provide no improvement on the standard comparison, better results are obtained using the integration method, when the above requirements are respected and profiles measured by PEARL at a time shift with respect to the overpass of CALIPSO are available (13 August 2006 case). This case shows a better result using the new method as compared to the older one. Thus, to confirm this result, a large number of case studies for which time-shifted PEARL measurements are available must be studied. Further improvement on the result should be obtained by substituting the root mean square error, which gives the same weight to all

layers between 2000 and 8000 meters, with a different and more appropriate kind of statistical analysis. The new method also constitutes a useful tool for determining whether CALIPSO and PEARL data can be employed to attain a direct intercomparison (when the arrival times are very short), or to gain a picture of the 4-D variability of aerosol distribution (when arrival times are long). Moreover, the new method provides the possibility of reconstructing an aerosol profile in a space-time point different from that of measurement.

4.2 Case study: ETNA eruption 2002

In this case study the eruption of Etna Volcano on October-November 2002 is considered. It is a standard case of aerosol transport in the atmosphere. In order to ascertain where the volcanic particles are transported different tools are used. Experimental measurements of the aerosol backscatter coefficient are available in Potenza for four different days, while estimates of column height over Etna for each day of the eruption are available from the Osservatorio di Catania. The Bol-Traj model is used here to relate the different types of information and to give an overview of the route of volcanic aerosol during the eruption. A similar study is made in (33), where the forward trajectories from Etna are examined to explain the experimental data in Potenza, and in (37), where different lidar measurements and several models are integrated in order to gain knowledge on volcanic aerosol transport on a continental scale . In the present work, the Bol-Traj model is used

1. in backward mode from Potenza, in order to establish the origin of the detected aerosol, and to obtain data for comparison with the estimates of columnar height of the Etna emissions (when the trajectories pass over the volcano)

2. in forward mode from Etna, to verify and confirm the backward simulation results.

4.2.1 Brief description of the eruption

Etna is located in Sicily (at longitude 15.10 latitude 37.75) and the crater is at 2750 m a.s.l. (1); the height of column of the plume is estimated for each day by combining barometric altimetry data with the analysis of images and videos captured from different viewpoints by the Osservatorio di Catania (1). The beginning of the eruption was marked by a seismic swarm that began on the evening of 26 October and lasted a few hours. From the beginning of the eruption explosive

activity occurred. During the first day of the eruption, a dense plume formed above the volcano as the two plumes originating from the NE and S fissures merged with the minor plumes rising from the summit. On the following days, the explosive activity at the S-fissure increased and the eruption column reached a maximum height of 7 km a.s.l (31 October). Intense lapilli and ash fallout began to cover the volcanic flanks, with finer ash reaching the northern African coast. Within a week, the explosive activity first began to decrease at both the summit craters and the NE-flank, stopping on 5 November. The explosive activity at the S-fissure was stronger and more continuous than at the NE-fissure, with eight main eruptive phases being recognized on the basis of intensity and eruptive style. From the onset of the eruption until 12 November, continuous fountaining activity started to build a cinder cone at 2750 m. Strombolian explosion occurred between 12 November and the evening of 13 November, when fire-fountains resumed at the cone and alternated with intense Strombolian activity. On 25 November an eruptive vent that was active during the first days of the eruption re-actived at 2800 m and gradually replaced the 2750 m vent as the primary activity source, so that a new cone started to grow and coalesce close to the lower cone. The violent activity at the 2800 m cone stopped between 8 and 10 December simultaneously with the re-activation of the 2750 m cone. From this date on a long waning phase began, characterized by less sustained and discontinuous explosive activity, which declined further in January, when only very moderate plumes formed at the 2750 m cone followed by minor effusive activity. The eruption definitively ended on 28 January 2003.

4.2.2 Starting point of trajectories: scheme of source

For the backward simulation of the Bol-Traj model the starting point of trajectories is considered the lidar backscatter profile measured at PEARL. The scheme of origin proposed is a vertical line and the trajectories start from the measurement points

Figure 4.27:

and time. For the forward simulation the Etna volcano is considered as the particle source: the scheme of source proposed is a vertical line; the particles are released with a uniform distribution between two extremes that vary according to the day. A subroutine extracts randomly the particles between the two fixed extremes.

4.2.3 End point of trajectories: scheme of detection

It is not necessary in this case study to write a special subroutine for the "arrival" of trajectories, because in backward mode the aim is to discover where the different lidar layers come from, while in forward mode it is to find out where the particles of SO_2 are heading. However, in order to establish whether the trajectories starting from Potenza arrive over Etna, and viceversa, it is sufficient to analyse in post-processing the output files, seeking the intersection between the point (longitude/latitude) representing the trajectory at each time step, and a domain surrounding the point of interest (Potenza in the forward case, and Etna in the backward case).

Figure 4.28:

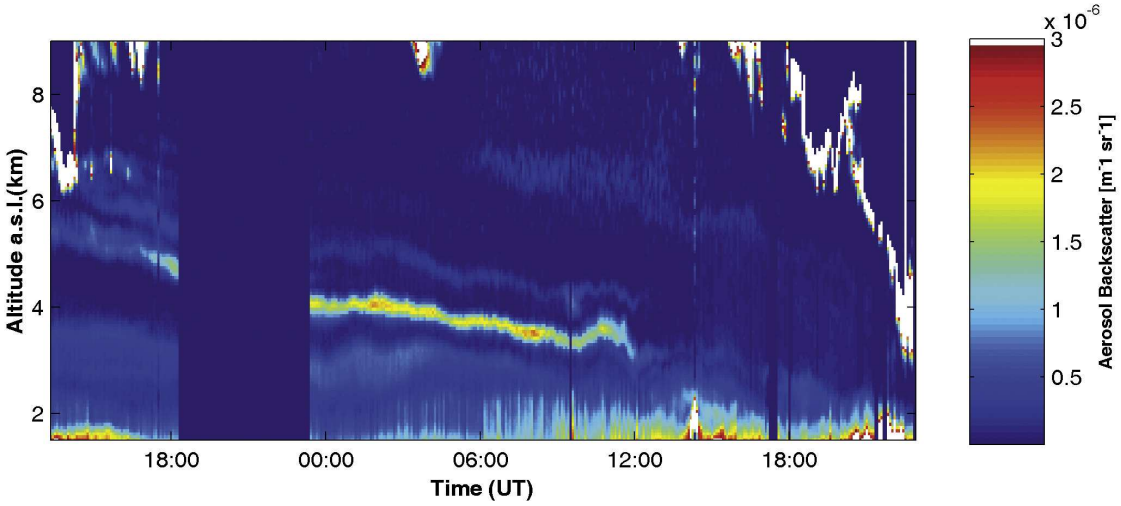

Figure 4.29: Case study: Etna eruption 2002. Aerosol backscatter coefficient

4.2.4 Simulations, Analyses and Results

case study: 1 November 2002

On 1 November 2002 in Potenza the lidar detected the presence of aerosol. Figure 4.31 shows the aerosol backscatter coefficient profile. It is supposed that different aerosol layers come from different geographic areas. The Bol-Traj backward simulation is used to verify this hypothesis and to ascertain the areas of interest. The lidar measurements are taken over Potenza (longitude 15.7 degree and latitude 40.6 degree) with vertical resolution of 60 meters between 2000 and 12000 meters and at time 23:35, which is the mean value between 23:20 and 23:50 (time interval of measurement integration used to obtain the profiles). A part of the trajectories, starting at between 3900-6100 meter altitude, move southward. Starting around 2:00 and continuing gradually until around 12:00, first the lower trajectories, followed by the ones at higher levels, pass over Mt. Etna at between 4200-5700 meters a.s.l. of altitude, as is shown in figure 4.38. This is in good agreement with observations of the Osservatorio di Catania, which affirm that the estimated top

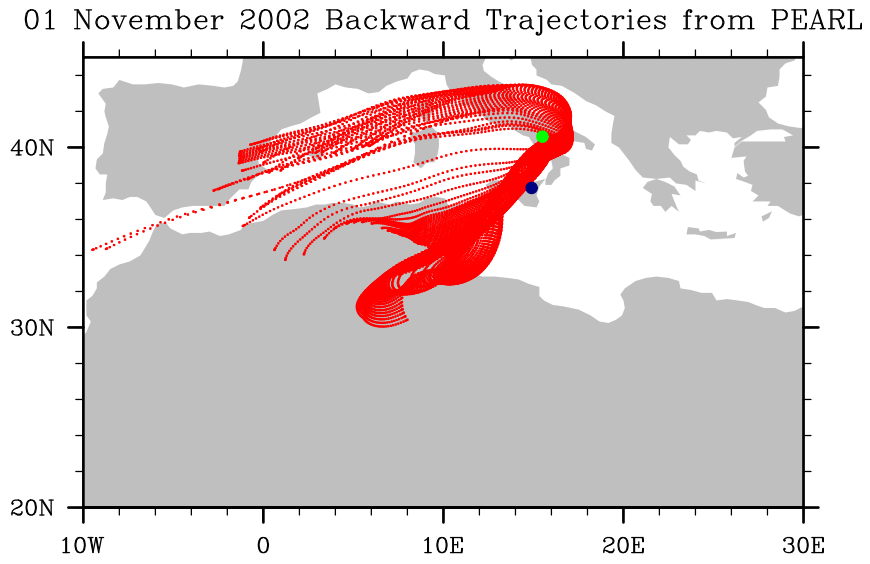

Figure 4.30: Case study: Etna eruption 2002. Backtrajectories from PEARL station

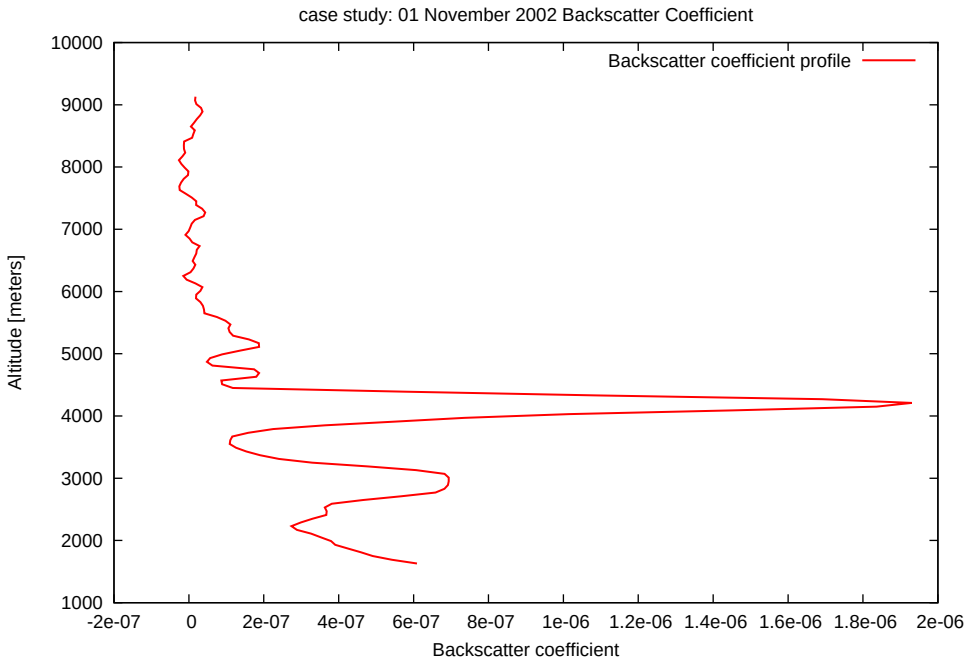

Figure 4.31: Case study: Etna eruption 2002. Backscatter coefficient measured in PEARL station

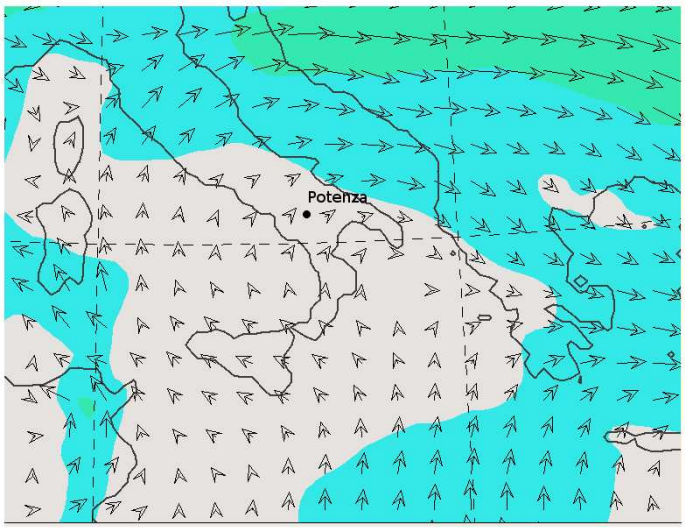

Figure 4.32: Case study: Etna eruption 2002. Plot of Wind fields at 500 hPa

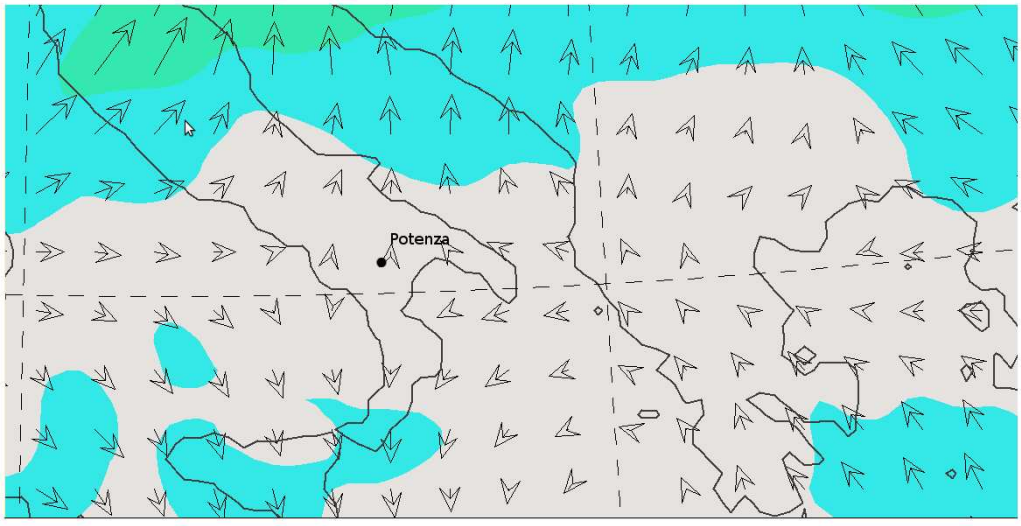

Figure 4.33: Case study: Etna eruption 2002. Plot of Wind fields at 700 hPa

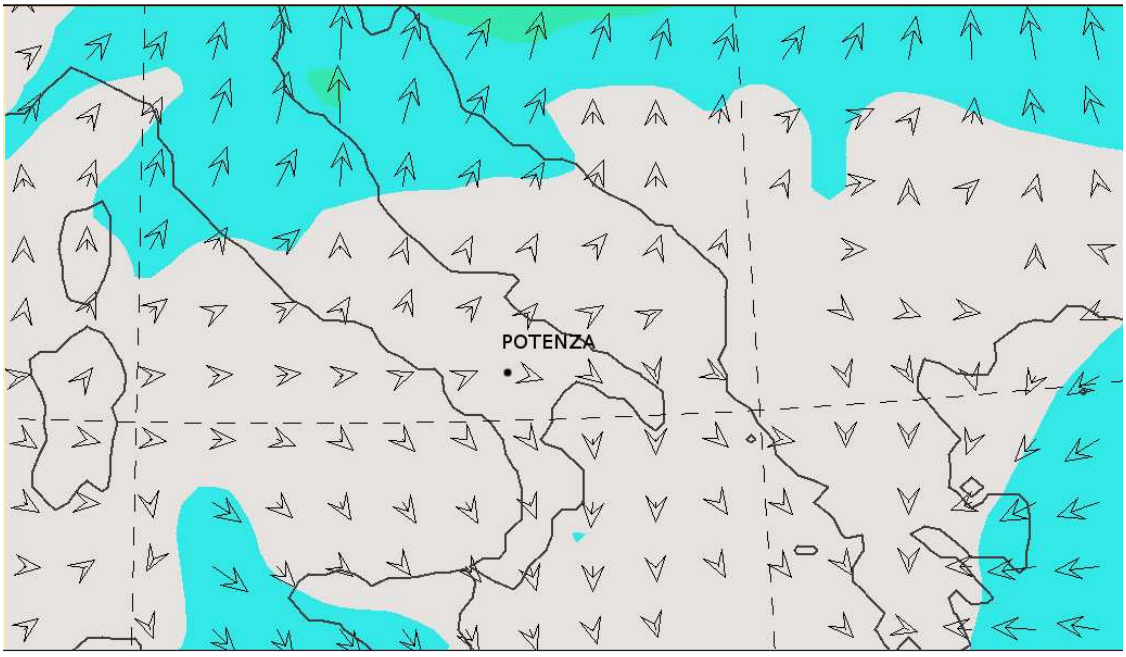

Figure 4.34: Case study: Etna eruption 2002. Plot of Wind fields at 850 hPa

of the SO_2 column over Etna was at 5700 meters a.s.l. and the bottom at 2750 meters a.s.l. (crater height) on 1 November (1). The layers of aerosol below 6100 meters in the PEARL profile arrive from the Saharan region, the trajectories being clearly visible over the Sahara area on 30 October, and passing in the vinicity of Etna on 1 November. By direct transport, the trajectories arrive over Potenza. It therefore reasonable to conclude that the layers above 6100 meters probably contain Saharan dust, with a small quantity of SO_2 found in the area surrounding the volcano in the days before 01 November. The lower layer of aerosol detected in Potenza, below 3900 meters, is transported from North-West, and comes from the recirculation of an anticyclonic circulation of the wind during the previous days, which was centered on the western Mediterranean, as shown in (33). Figures 4.35 and 4.36 are the same as above, but the different regions found are marked by three different colours.

The altitudes of trajectory arrival are confirmed by a cross-check. Using the

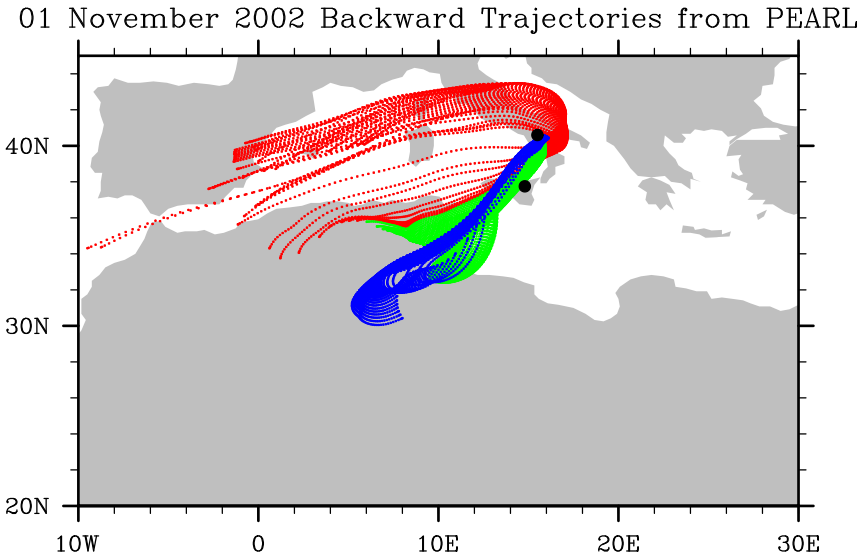

Figure 4.35: Case study: Etna eruption 2002. Backtrajectories from PEARL station: different colours underline different aerosol provenience

Bol-Traj model in forward mode, an ensemble of trajectories is started from Etna (longitude 15.10 degree and latitude 37.75 degree) with height between 2750 and 5700 meters a.s.l. at 12:00. The trajectories pass over Potenza around the measurement time at height between 5800 and 6100 meters, as shown in figure 4.37. The discrepancy between the altitude over Potenza (3900-6100 for backward simulation and 5800-6100 for forward simulation) is explained by the different arrival times of the trajectories. In fact, the forward simulation concerns a start time over Etna and the time stop over Potenza that coincides with the time of measurement, while backward simulation considers the start time over Potenza (time of measurement) but no specific stop time over Etna. This is confirmed by the results of the forward simulation: around 12:00 the trajectories that start from Etna between 5400 and 5600 meters, arrive over Potenza at between 5800 and 6100 meters at the measurement time.

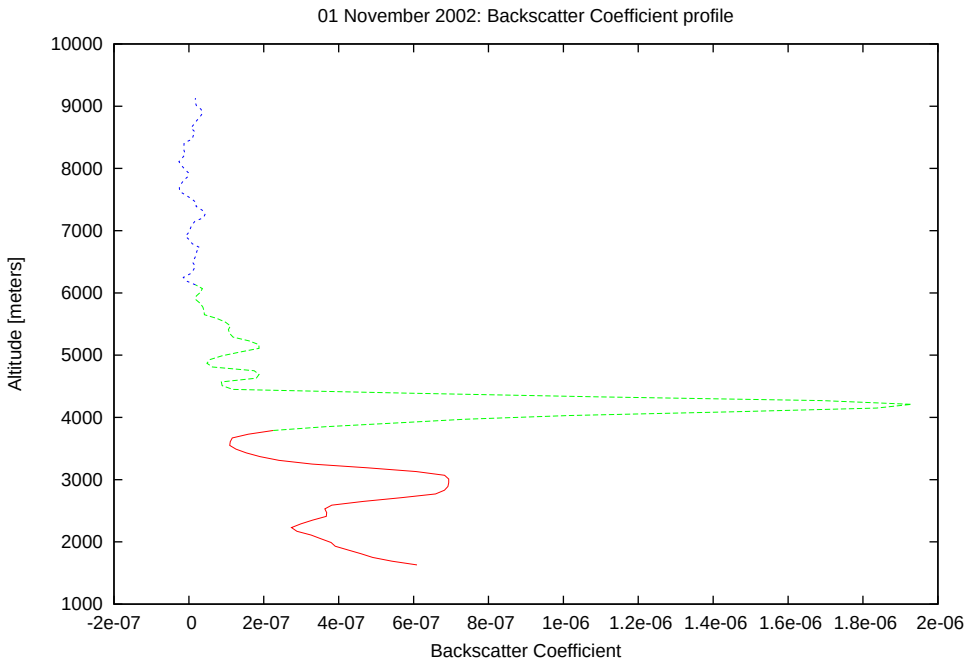

Figure 4.36: Case study: Etna eruption 2002. Backscatter coefficient measured in PEARL station: different colours underline different aerosol provenience

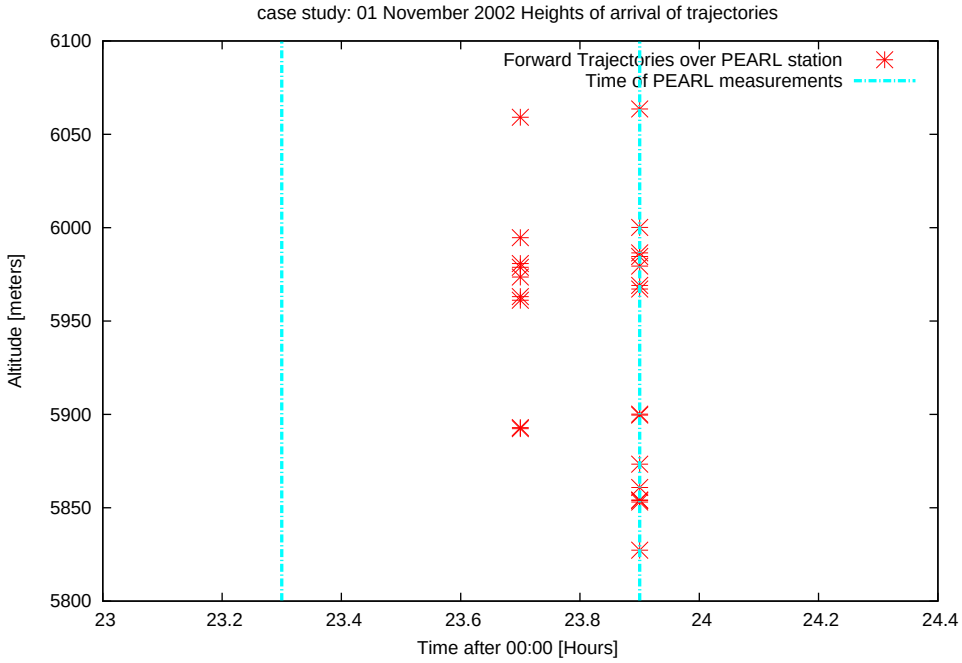

Figure 4.37: Case study: Etna eruption 2002. Height and time of forward trajectory arrivals over PEARL station coming from Etna volcano.

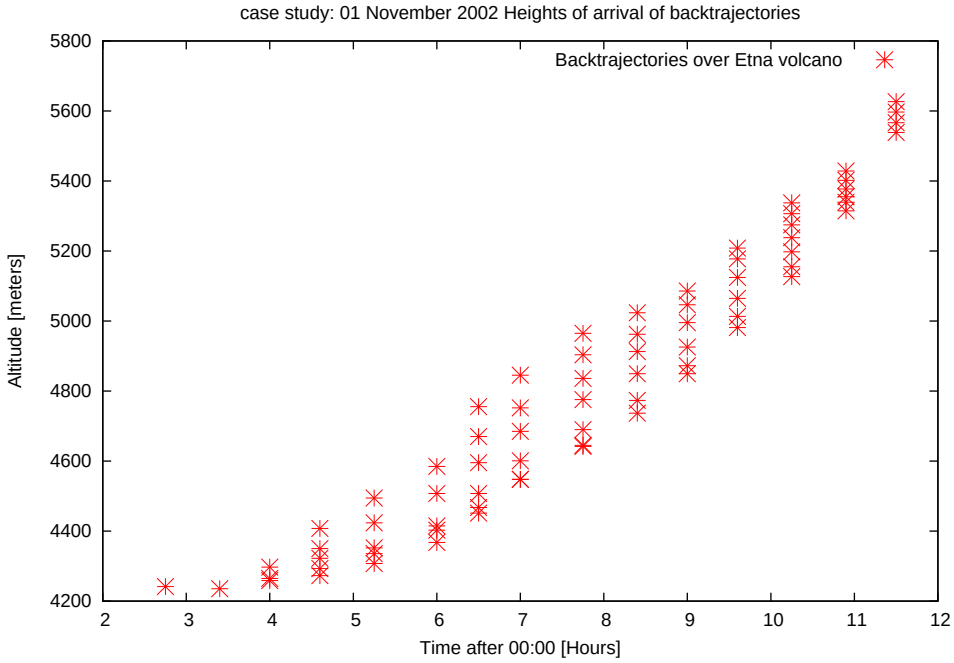

Figure 4.38: Case study: Etna eruption 2002. Height and time of backtrajectory arrivals over Etna volcano station coming from PEARL station.

4.2.5 Summary of results

The Etna eruption is dealt with in this case study. Information supplied by the backward trajectories of the Bol-Traj model from Potenza, the forward trajectories from Etna, plume height estimates from the Osservatorio di Catania, and lidar measurements at the PEARL station, is integrated to acquire a detailed knowledge on the transport of aerosol during the 2002 eruption. Compared to (33), a better estimate of the Etna source height is considered (1), and the backward simulation is introduced to provide different information with respect to the forward. The forward simulation is a tool that shows the displacement of aerosol emitted by Etna and is useful for reconstructing the plume, while the backward simulation determines the origins of the aerosol detected at PEARL, including non-volcanic aerosol. In the present work the forward simulation is used merely to confirm the results of the backward simulation, and to link the information of the Osservatorio di Catania with those from PEARL. Judging by the height and time of trajectory arrival over Potenza and over Etna, it is possible to affirm that the results are in good agreement.

4.3 Case study: Forest Fires August 2007

In this case study different kinds of measurements integrated with the dispersion model are used. The aim is to obtain a better knowledge of forest fire aerosol transport.

Fires contribute substantial emissions of trace gases and particles to the atmosphere, which can impact air quality and even climate. Fires emit a variety of gases and aerosols to the atmosphere, including carbon dioxide CO_2, carbon monoxide CO, nitrogen oxides NO_x, volatile and semivolatile organic compounds VOC and $SVOC$, particulate matter PM, ammonia NH_3, sulfur dioxide SO_2, and methane CH_4. As gaseous and aerosol emissions from fires are transported through the atmosphere, they degrade air quality by reducing visibility, creating unhealthy levels of PM, and reacting to create harmful tropospheric trace gases, such as ozone 0_3. An important task of this case study is to estimate the height of emissions. Even though a few methods have been proposed for this purpose, emission plume height is still not well quantified. In (38), for example, a method for estimating the emissions from fires is presented and applied in North and Central America (10-71 N and 55-175 W), taking advantage of a combination of complementary satellite and ground-based data to refine estimates of fuel loadings. Here, the integration between the Bol-Traj model, PEARL lidar measurements and MODIS maps is carried out in order to estimate the height of the plume. The MODIS Rapid Response System was developed to provide daily satellite images of the Earth's landmasses in near real time. True-color, photo-like imagery and false-color imagery are available within a few hours of being collected, making the system a valuable resource for organizations like the U.S. Forest Service and the international fire monitoring community.

The method consists of two steps:

1. Use of MODIS maps to locate (longitude and latitude) the forest fires in Algeria on 29 August 2007

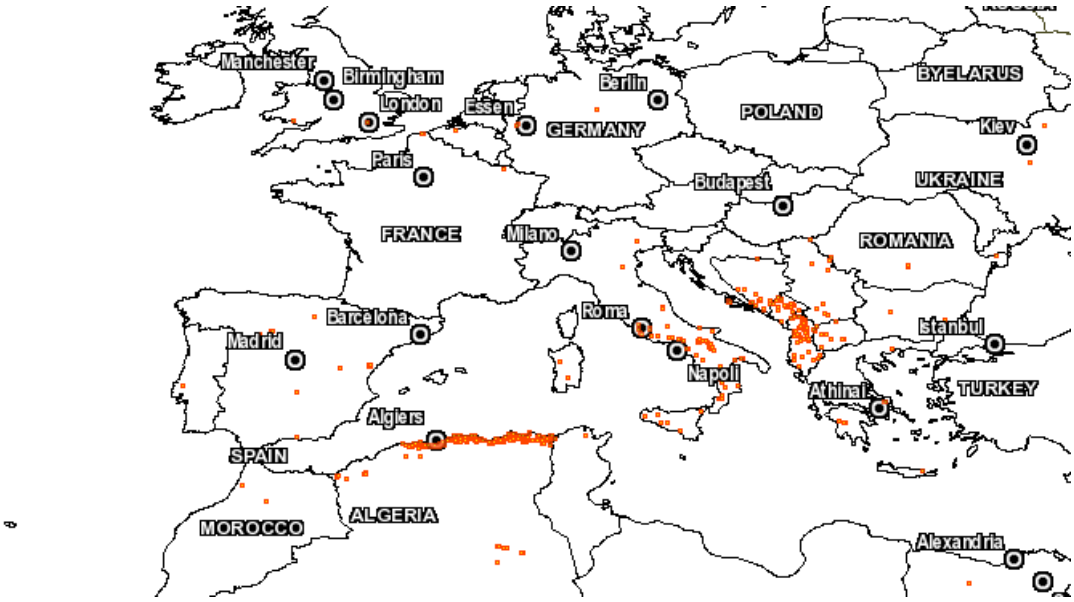

Figure 4.39: Case study: Forest Fires 2007. MODIS map of fires on 29 August 2007

2. Use of PEARL measurements (backscatter coefficient and lidar ratio) on 30 August with backtrajectories of the Bol-Traj model to obtain an estimate of plume height in Algeria: an ensemble of backtrajectories transported by the Bol-Traj model are started over Potenza at the presumed height of typical fire aerosol at time of measurement; when they pass over a forest fire, which is located by knowing the longitude and latitude on the MODIS map, an evaluation of the plume height is possible.

4.3.1 Starting point of aerosols: scheme of source

The start of trajectories is the PEARL station. The scheme of origin proposed, in this case, is a vertical line and the trajectories start in the measurement point of the PEARL station, where a layer of typical fire aerosol is hypothesised by integrating

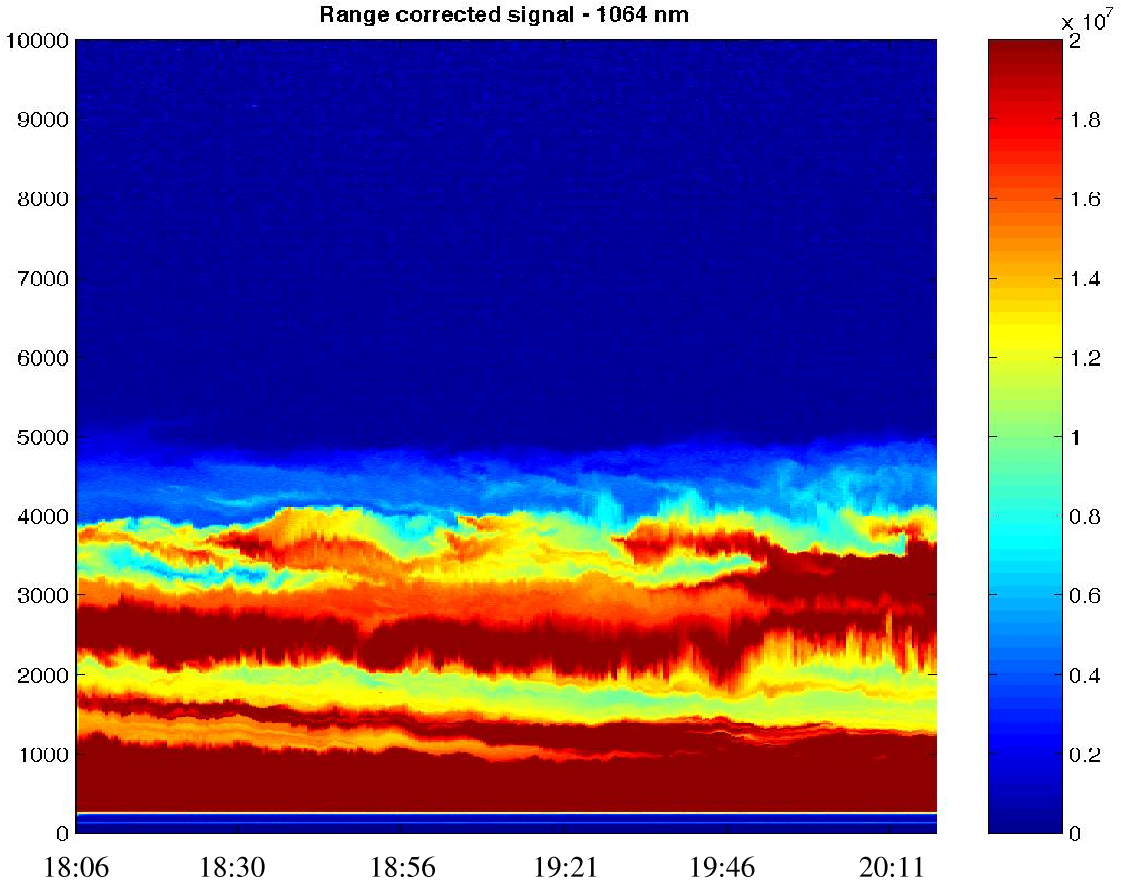

Figure 4.40: Case study: Forest Fires 2007. Backscatter coefficient measured in PEARL station.

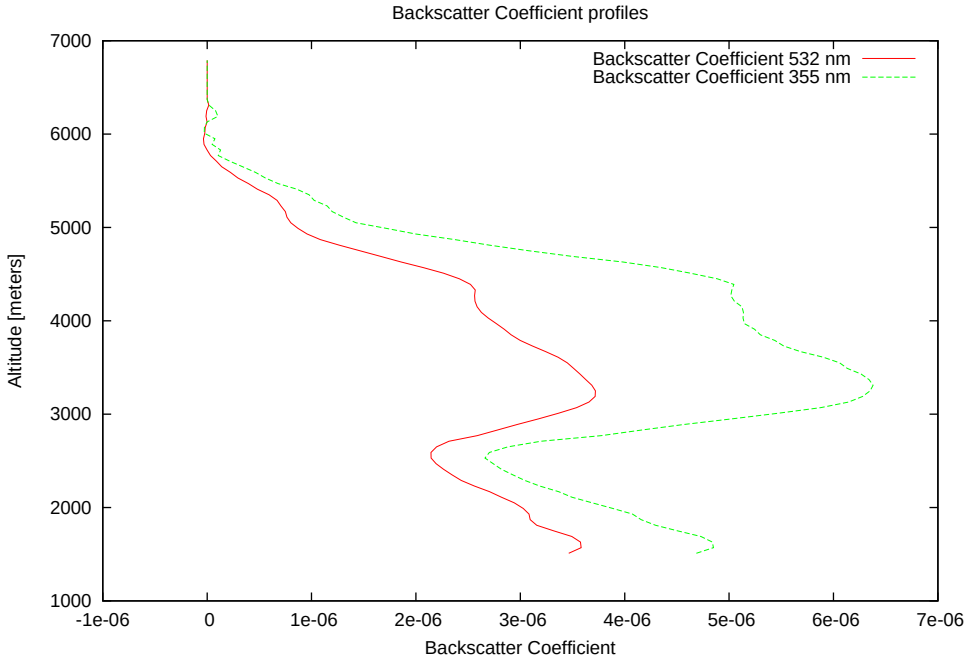

Figure 4.41: Case study: Forest Fires 2007. Backscatter profiles measured in PEARL station.

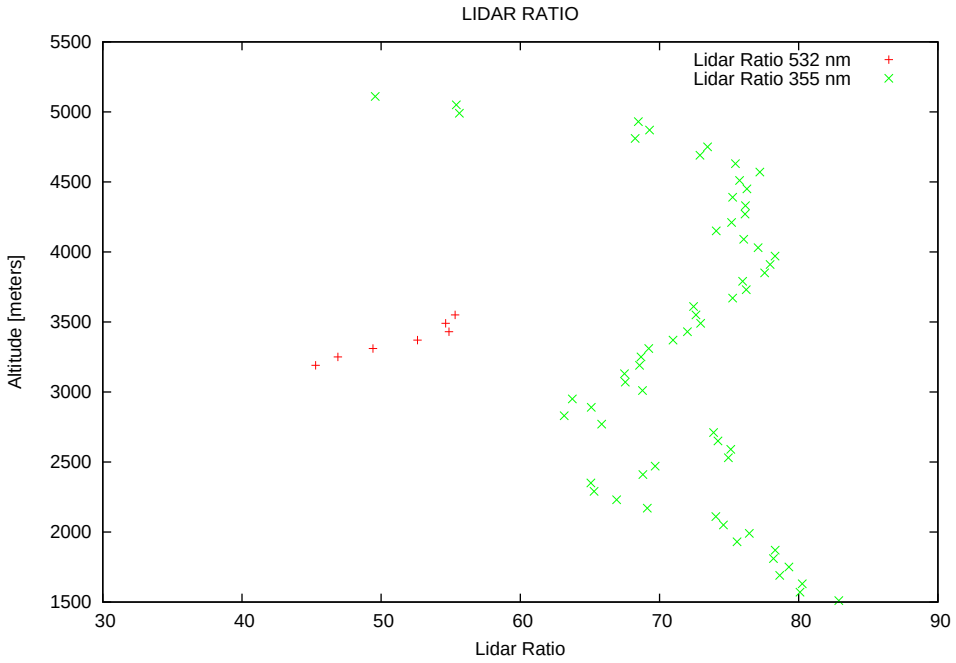

Figure 4.42: Case study: Forest Fires 2007. Lidar Ratio profiles measured in PEARL station.

4.3.2 End point of trajectories: scheme of detection

It is not necessary in this case study to write a special subroutine for the "arrival" of trajectories, but in order to find out whether the trajectories starting from Potenza arrive over the forest fires, and then make an estimation of the plume height, it is sufficient to analyse in post-processing the output files. The aim is to find the intersection at every time step between the points representing the trajectories and the small domain surrounding each forest fire.

4.3.3 Simulations, Analyses and Results

case study: 29 August 2007

An unusual layer of aerosol is detected by the PEARL station lidar on 30 August 2007 above 4800 meters of altitude. Figure 4.40 shows the lidar observation. The backscatter coefficient is a measurement of the light backscattered by particles, and the lidar ratio, the ratio between the extinction coefficient and backscatter coeffient, where the extinction coefficient is a measurement of the light extinguished by scattering and absorption. These coefficients depend on the shape and size of the particles. By measuring these optical properties at different wavelengths, it is possible to formulate some hypotheses on the kind of aerosol detected. The lidar ratio measured between boundary layer and 4800 metres assume a value of 70 sr, which is untypical of Saharan dust events. In addition, the Eulerian DREAM model reveals that no Saharan dust events are in progress, while the lidar ratio values are untypical for the period. Therefore, the aerosol layer between the boundery layer and 4800 meters is hypothesised to contain the typical aerosol characteristic of the forest fire period.

The simulation starts on 31 August 2007 at 00:00 and stops on 29 August 2007 at 00:00, after the passage of the trajectories over Algerian forest fires. The wind fields are available every 20 km, every 1 hour, and the linear interpolation, as described in chapter 2, is made in order to obtain the wind fields every 180 sec. The backtrajectories start on 30 August 2007 at 18:50 (mean time between the times of start and stop of measurement), at the measurement points that have 60 meters of resolution in 105 levels along the vertical. The work of post-processing of the output file consists of two steps:

1. identify the trajectories that pass over each forest fire using the longitude and latitude coordinates from the MODIS map

2. when a trajectory passes over a forest fire, retrieve the time of overpass,

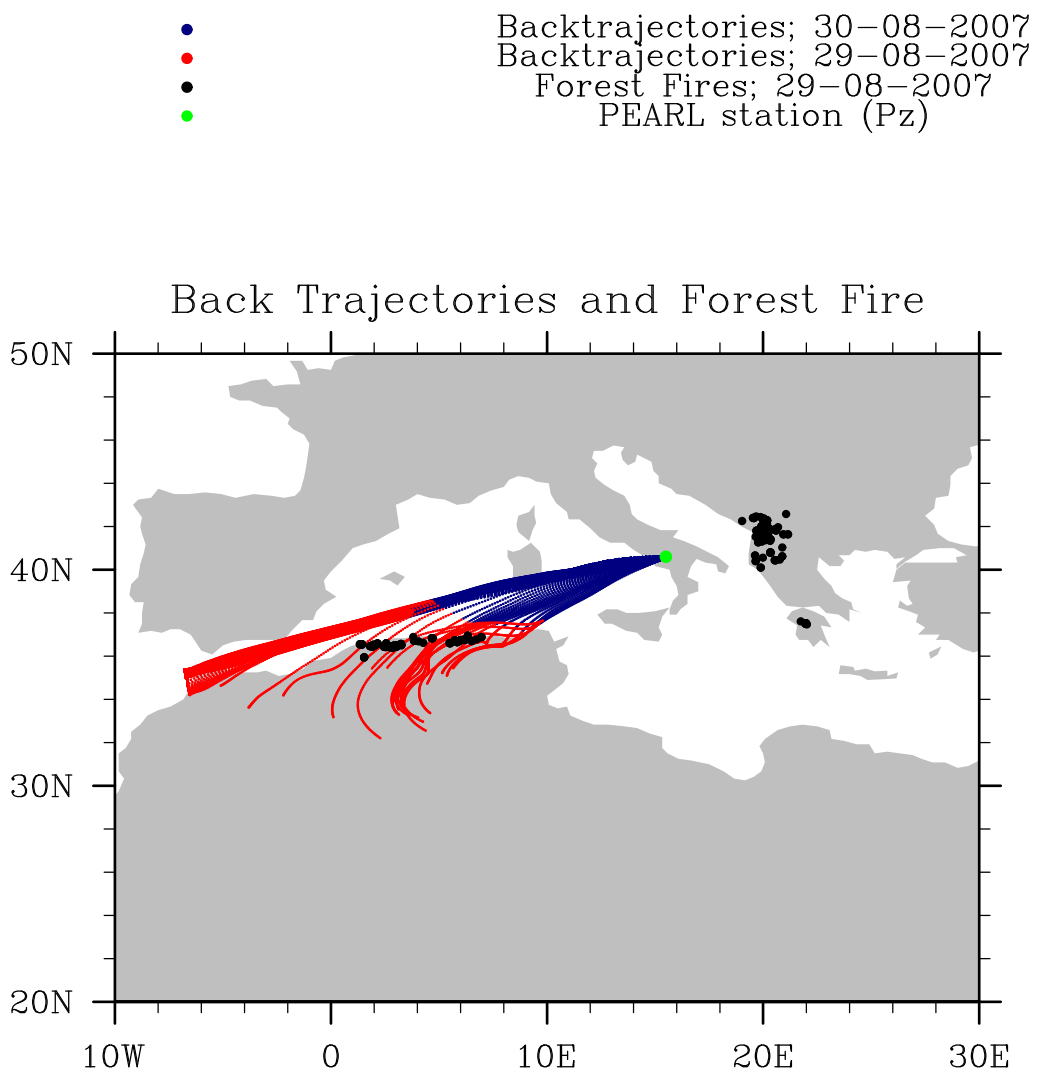

Figure 4.43: Case study: Forest Fires 2007. Backtrajectories from PEARL station.

the trajectory index, which is important to locate the height of the origin, and, finally, the plume height over longitude and latitude point of the fire, recording these data in an output file.

The results are shown in tab 4.1, where the first two columns are the longitude and latitude, respectively, of the point at which the estimation of emission is possible, the third column is the plume height, and the fourth the time at which it is possible to estimate the plume height.

Table 4.1: Table of longitude, latitude, height estimation and time of estimation for each forest fire

LONGITUDE	LATITUDE	ALTITUDE	TIME
1.478561	36.49372	2193.920	16:30
2.865502	36.34938	1730.760	03:30
2.951883	36.41156	1667.400	03:45
3.041549	36.47129	1584.710	04:00
3.228914	36.58431	1389.510	04:30
3.237717	36.46544	2294.580	17:45
3.759662	36.90751	2002.610	19:30
3.839919	36.87096	1171.890	06:00
4.034616	36.66607	1650.150	05:15
4.723092	36.82212	1626.900	19:45
5.497310	36.58702	2778.510	18:15
5.674570	36.67598	2677.430	18:45
5.759006	36.71892	2635.500	19:00
6.294048	36.97566	1250.720	08:00
8.722342	36.80372	2130.730	19:45
8.725175	36.98708	1833.190	22:45
8.730931	36.97464	1855.130	18:15

LONGITUDE	LATITUDE	ALTITUDE	TIME
8.750554	36.82056	2093.710	20:00
8.752919	37.01901	1802.620	23:00
8.765098	36.98138	1840.330	18:30
8.779714	36.83797	2057.480	20:15
8.780603	37.05251	1775.390	23:15
8.798259	36.98862	1825.090	18:45
8.807186	36.85589	2020.940	20:30
8.810255	37.08749	1750.180	23:30
8.830980	36.99634	1808.950	19:00
8.836871	36.87446	1983.540	20:45
8.839288	37.12387	1728.270	23:45
8.862945	36.89383	1945.060	21:00
8.865830	37.00478	1793.370	19:15
8.870279	37.16155	1712.320	00:00*
8.891648	36.91412	1903.070	21:15
8.895322	37.01426	1774.860	19:30
8.905128	37.20027	1701.520	00:15*
8.916071	36.93543	1860.720	21:30
8.925982	37.02484	1755.080	19:45
8.947661	36.95796	1819.860	21:45
8.965736	36.98185	1781.300	22:00
8.965736	37.03660	1734.460	20:00
9.000000	37.04952	1713.180	20:15
9.019783	37.00730	1744.070	22:15
9.027977	37.03447	1708.110	22:30
9.027977	37.06365	1690.610	20:30

LONGITUDE	LATITUDE	ALTITUDE	TIME
9.055953	37.06324	1674.790	22:45
9.059347	37.07912	1666.640	20:45
9.083930	37.09575	1642.090	21:00
9.086229	37.09319	1645.160	23:00
9.111906	37.12428	1618.160	23:15
9.117034	37.11337	1615.800	21:15
9.144018	37.15651	1593.150	23:30
9.146710	37.13179	1587.890	21:30
9.174713	37.18998	1571.560	23:45
9.178041	37.15113	1559.420	21:45
9.209357	37.17156	1532.020	22:00
9.243894	37.19315	1505.280	22:15

The results between 16:45 and 19:15 are shown in figure 4.44, where different colours indicate the different ranges of emission height.

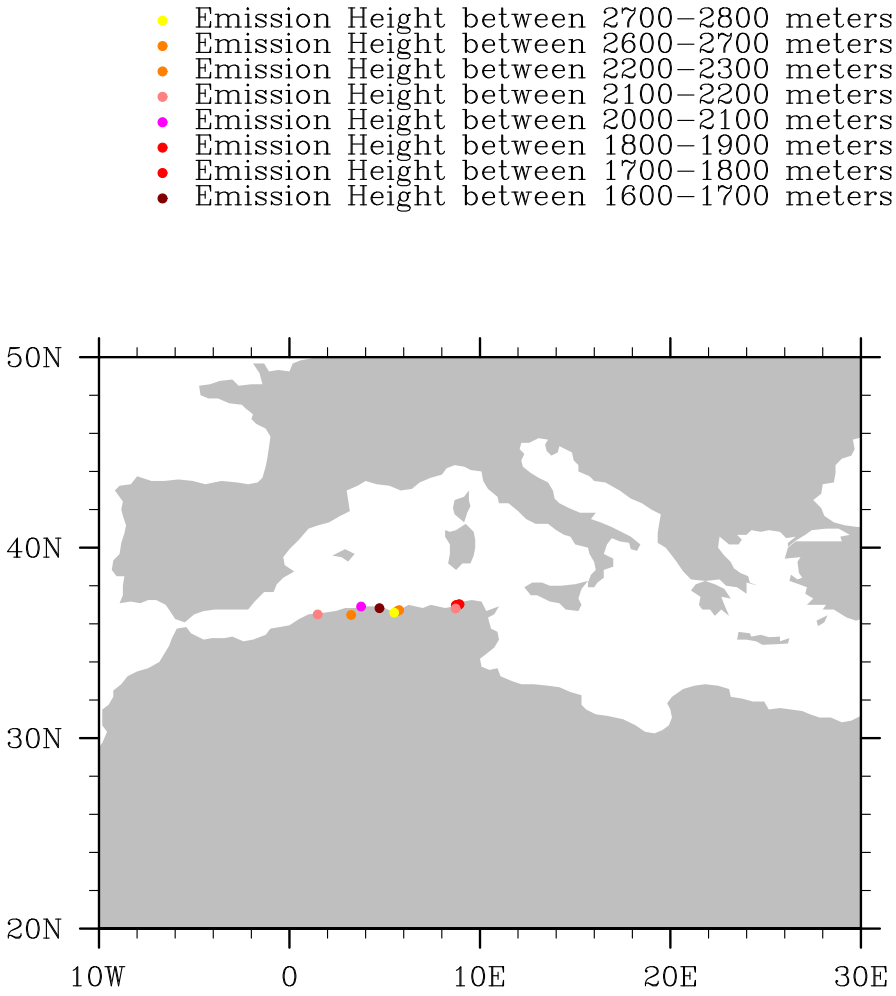

Figure 4.44: Case study: Forest Fires 2007. Estimation of forest fire plume heights: different colours represent different range of altitude

4.3.4 Summary of results

The aim of the integration between experimental measurements and theoretical models in this case study is to determine the plume height of the forest fire in Algeria in 29 August 2007. To attain this goal, two different instruments (MODIS and PEARL) are used, adopting Bol-Traj as theoretical model. Applying some experimental hypotheses on the data measured at the PEARL station, an unusual layer of aerosol is identified. The backward trajectories of the Bol-Traj model transport the identified layer back in time. The MODIS spectrometer maps supply the longitude-latitude coordinates of the forest fires. In post-processing, the route followed by particles coming from Potenza is analysed and is set in relation to the horizontal coordinates of the MODIS map. Because the trajectories are computed in 4-Dimensions (1 for time, 3 for space), it is possible to estimated the plume height at the longitude/latitude points of the MODIS map when the trajectories pass over the fire. Table 4.1 summarises the results. The first two columns report the longitude and latitude, respectively, of the fire, the third is the estimated plume height, and the fourth is the estimation time. The results are in good agremeent with the heights found by (22) ISAC, Lecce, who used the Eulerian model BOLCHEM, comparing the results with PEARL data, and estimated the plume height to be in the [1500-3000] meter range. A useful tool that could be employed to obtain independent estimates of the same fire, at either the same or different times, is CALIPSO aerosol data, when available. On 29 August the CALIPSO groundtrack was up-wind to respect the fires, for this reason it was impossible to also include this tool. It would also be interesting to set the heights found by the present method as the sources in the Eulerian model BOLCHEM, to obtain the aerosol concentrations coming from forest fires at grid points, and, subsequently, compare them with the concentration data measured at Monte Cimone at the ground.

Conclusions

Over recent years scientific research has thrown light on the need to study the transport of aerosol in the atmosphere. The importance of gaining an improved knowledge on this issue is summarized in the three major points underscored in the Introduction.

To investigate atmospheric aerosol transport, two different methods are appropriate: transport models and experimental measurements. At the present time, a wide range of transport models and many typologies of experimental instruments exists. However, the most accurate way to analyse aerosol transport is by using both types of method in concert. For this purpose, a new Lagrangian dispersion model Bol-Traj is developed and proposed in this work. The advantage of using the Bol-Traj model lies in the fact that it is applicable to a large number of case studies, because it requires the parameterization of the origin and destination trajectories. This feature is of considerable importance because, after an a priori study of the case, it permits an optimum treatment of the aerosol source. A further important characteristic of the model is that it runs on-line with the limited area meteorological code, which provides the opportunity to select the model's resolution as required, as well as reducing computational costs.

The new model is integrated with different measurement instruments, CALIPSO, PEARL, and MODIS, and applied to three case studies.

1. The first case study, CALIPSO-PEARL, shows that integration allows a comparison between two space-time different measurements. Currently, an

existing method provides a direct comparison between profiles measured by spaceborne lidars and those measured by ground-based lidar, whereas the newly developed method integrates the dispersion model with the two kinds of measurements to reach the same aim. The new method is found to give better results than the older one, but many further case studies are need to confirm the results obtained.

However, the usefulness of the new method is not limited to making comparisons between different space-time measurements. It is a very important tool for the reconstruction of aerosol profiles at space-time points different from the measurement point. It therefore provides a 4-D structure of the aerosol distribution in the atmosphere, which at present constitutes an original and interesting result.

2. The second case study, the Etna eruption of 2002, is a typical investigation of aerosol transport in the troposphere. In this case, the integration between the dispersion model and lidar measurements and the estimated eruption height supplied by the Osservatorio di Catania, allowed the discovery of the origin of different aerosol layers detected by the lidar. The model is used in backward and forward mode, the first in order to reach the mentioned objective, the second in order to confirm the results of the backward simulation. The results of two simulation are in good agreement with each other and with the plume height estimates of the Osservatorio di Catania. The latter point is of considerable interest, because the method, as well as constituting a useful tool for the determination of the origin of aerosol layers, also offers the opportunity of obtaining independent plume height estimates during an any eruption.

3. The third case study, Forest Fire 2007, described a method that integrates the dispersion model with longitudinal/latitudinal maps supplied by satellite

spectroradiometer and lidar measurements, to provide the plume height of the forest fire. The results are in good agreement with the rougher estimate of the plume height range made by ISAC Lecce, based on a Eulerian model and a comparison with lidar measurements. To obtain independent plume height estimates at the same and different times of a forest fire, the use of alternative measurements, for example spacesborne lidar, integrated with the Lagrangian dispersion model is recommended. An important development of this case study is the use of a Eulerian model, in which the heights of emission sources are the those supplied by this work. The results of a Eulerian simulation are the aerosol concentrations at grid points. These could be compared with ground level aerosol concentrations measured at Monte Cimone station, in order to obtain an estimate of 4-D aerosol distribution coming from forest fires.

Acknowledgement

I thank my tutors Dott. Gelsomina Pappalardo and Dott. Alberto Maurizi for the opportunity that they gave me to produce this work. I also wish to thank all my colleagues of the institutes IMAA-CNR of Potenza and ISAC-CNR of Bologna, for their material and psychological support. I am grateful to the Osservatorio di Catania for the data supplied and to ISAC-CNR Lecce for their collaboration. Very special thanks go to all my family for all their support and patience. Finally, I extend special thanks and gratitude to everyone who believed and still believes in me.

Bibliography

[1] D.Andronico, S.Scollo, S.Caruso, A. Cristaldi, The 2002-03 Etna explosive activity: Tephra dispersal and features of the deposits, Journal of Geophysical Research, Vol. 113, B04209, doi:10.1029/2007JB005126, 2008

[2] J. Brandt, J. H. Christensen, and L. M. Frohn, Modelling transport and deposition of caesium and iodine from the Chernobyl accident using the DREAM model (2002) Atmos. Chem. Phys.

[3] E.Chianese,G.Giunta, A.Riccio, Application of a trajectory classification procedure to interpret the transport of atmospheric pollutants in the urban area of Naples (Southern Italy)

[4] Carn S. A., Prata A. J., Karlsdottir S., Circumpolar transport of a volcanic cloud from Hekla (Iceland) (2008) Journal of geophysical research

[5] K.Doty, D.Perkey, Sensitivity of trajectory calculations to the temporal frequency of wind data, American Meteological Society 1992

[6] R.R.Draxler, Sensitivity of a trajectory model to the spatial and temporal resolution of the meteorogical dara during CAPTEX, Amrican Meteorological Society, 1987

[7] M. D'Isidoro, A. Maurizi, F. Tampieri, A. Tiesi, M. G. Villani, Assessment of the numerical diffusion effect in the advection of a passive tracer in

BOLCHEM, IL NUOVO CIMENTO vol. 28 C, N. 2 DOI 10.1393/ncc/i2005-10188-y 2005

[8] Draxel R. R., Taylor A. D., Horizontal dispersion parameters for long-range transport modelling (1982) J. Appl. Meteorol.

[9] T.J.Duck, B.J.Firanski, D.B. Millet, A.H. Goldstein, J. Allan, R. Holzinger, D.R. Worsnop, A.B. White, A. Stohl, C.S. Dickinson, A. van Donkelaar, Transport of forest fire emissions from Alaska and the Yokon Territory to Nova Scotia during summer 2004, Journal of Geophysical Research, vol. 112, D10S44, doi:10.1029/2006JD007716, 2007

[10] S. Eckhardt, AJ Prata, P.Seibert, Estimation of vertical profile of sulfur dioxide injection into the atmosphere by a volcanic eruption using satellite column measurements and inverse transport modeling, Atmospheric Chemistry and Physics, 8(14): 3881-3897 2008

[11] Flesch T.K., Wilson J.D., Backward-time lagrangian stochastic dispersion models and their application to estimate gaseous emissions J. App. Met.

[12] F. Gheusi, J. Stein, Lagrangian description of airflows using Eulerian passive tracers Q.J.R. Meteorol. Soc. 2002, 128, pp. 337-360

[13] J.D.W.Kahl, On the prediction of trajectory model error, Atmospheric Environment Vol. 30 No.17, pp.2945-2957, 1996

[14] T. Kovacs, Comparing MODIS and AERONET aerosol optical depth at varying separation distances to assess ground-based validation strategies for spaceborne lidar, 2006, Journal of Geophysical Research, Vol 111, doi:10.1029/2006JD007349

[15] I. Lagzi , D. Karman, T. Turanyi , A.S. Tomlin , L. Haszpra , Simulation of

the dispersion of nuclear contamination using an adaptive Eulerian grid model (2004) Journal of Environmental Radioactivity

[16] T.Y.Lee, S.W.Park, S.B.Kim, Dependence of trajectory accuracy on the spatial and temporal densiteis of wind data, Tellus 49B (1997), 2

[17] L. Mona, A. Amodeo, G. DAmico, G. Pappalardo First comparisons between CNR-IMAA multi-wavelength Raman lidar measurements and CALIPSO measurements

[18] L. Mona, G. Pappalardo, A. Amodeo, G. DAmico, F. Madonna, A. Boselli, A. Giunta, F. Russo, V. Cuomo One year of CNR-IMAA multi-wavelength Raman lidar measurements in correspondence of CALIPSO overpass: Level 1 products comparison

[19] L. Mona, Studio di aerosol atmosferici mediante tecniche ottiche di remote sensing (2003) Tesi di dottorato di ricerca in Fisica Universit di Salerno

[20] R. C. Owen, R. E. Honrath, Technical Note: A new method for the Lagrangian tracking of pollution plumes from source to receptor using gridded model output, 2008, Atmos. Chem. Phys. Discuss., 8, 18843-18891

[21] C.Perez, S.Nickovic, J.M.Baldasano, M.Sicard, F.Rocadenbosch, V.E.Cachorro A long Saharan dust event over the western Mediterranean: Lidar, Sun photometer observations, and regional dust modeling, 2006 Journal of Geophysical Research, Vol 111, D15214, doi:10.1029/2005JD006579

[22] C. Pizzigalli, Poster presented on PM 2008 Convegno nazionale sul particolato atmosferico 6-8 October

[23] S. Scollo, A. Folch, A. Costa, A parametric and comparative study of different tephra fallout models Journal of Volcanology and Geothermal Research 176 (2008) 199-211

[24] C. Schar, H. Wernli, Structure and evolution of an isolated semi-geostrophic cyclone, Q.J.R.Meteorol.Soc (1993), 119, pp.57-90

[25] C.H.Song, K.M.Han, H.J.Cho, et al., A Lagrangian model investigation of chemico-microphysical evolution of northeast Asian pollution plumes within the MBL during TRACE-P, Atmospheric environment, 41 (39):8932-8951 DEC 2007

[26] Stohl A., The flexpart particle dispersion model Version 5.0 (User guide)

[27] A.Stohl, Computation, accuracy and applications of trajectories - A review and bibliography, Atmospheric Environment Vol.32 No.6, pp.947-966, 1998

[28] A.Stohl, P.Seibert, Accuracy of trajectories as determined from the conservation of meteorogical tracers, Q.J.R.Meteorol.Soc. (1998), 124, pp.1465-1484

[29] Stohl A., Thomson D.J., A density correction for lagrangian particle dispersion models

[30] A.Stohl, G.Wotawa, P.Seibert, H.Kromp-Kolb, Interpolation errors in wind fiels as a function of spatial and temporal resolution and their impact on different types of kinematic trajectories, American Meteorological Society 1995

[31] Z.Tao, M.P. McCormick, D.Wu A comparison method for spaceborne and ground-based lidar and its application to the CALIPSO lidar Appl. Phys. B 91, 639644 (2008), DOI: 10.1007/s00340-008-3043-1

[32] D.J.Thomson, Criteria for the selection of stochastic models of particle trajectories in turbulent flows, J. Fluid Mech (1987) vol. 180 pp. 529-556

[33] G.Villani,L.Mona, A.Maurizi, G.Pappalardo, A.Tiesi, M.Pandolfi, M,D'Isidoro,V.Cuomo, F.Tampieri, Transport of vulcanic aerosol

in the troposphere:The case study of 2002 Etna plume, Journal of Geophysical Research, Vol 111, D21102, doi:10.1029/2006JD007126, 29006

[34] M.Wenig, N.Spichtinger, A.Stohl at al., Intercontinental transport of nitrogen oxide pollution plumes, Atmospheric Chemistry and Physics, 3:387-393 APR 3 2003

[35] .Wiedinmyer, B.Quayle, C.Geron, A.Belote, D.McKenzie, X.Zhange, S.O'Neill, K.Klos Wynne, Estimating emissions from fires in North America for air quality modeling ATMOSPHERIC ENVIRONMENT (2006)

[36] Wilson J.D., Sawford B.L., Review of lagrangian stochastic models for trajectories in the turbulent atmosphere (1995)

[37] X. Wanga, A. Boselli, L. DAvino, G. Pisani, N. Spinelli, A. Amodeo, A. Chaikovsky, M. Wiegner, S. Nickovic, A. Papayannis, M.R. Perrone, V. Rizi, L. Sauvage, A. Stohl Volcanic dust characterization by EARLINET during Etnas eruptions in 20012002, Atmos. Environment (2007)

[38] C. Wiedinmyer, B. Quayle, C. Geron, A. Belote, D. McKenzie, X. Zhange , S. O'Neill, K. Klos Wynne, Estimating emissions from fires in North America for air quality modeling, Atmospheric Environment 40 (2006) 3419-3432

[39] Winker D.M., W. Hunt, and M. McGill, "Initial perfomance assessment of CALIOP", (2006) Geophys. Res. Lett.

[40] D.M. Winker, J. Pelon, M. P. McCormick, The CALIPSO mission: Spaceborne lidar for observation of aerosols and cloud